Experimental investigation of the Combustion Efficiency of 4" to 14" Pipe Flares

Lartigue G.[b,a,*], Buzlukov A.[b], Daniel J.[b], De Decker T.[b], Dugué J.[b], Houzay E.[b], Klahr D.[b], Lenninger M.[c], Baranger P.-A.[d], Kretzschmar S.[e], Withnall R.[e], Ferrante A.[f], Saponaro A.[f], Scarano A.[f]

[a] *CORIA, CNRS UMR-6614, INSA de Rouen, Universite de Rouen, Saint-Etienne-du-Rouvray, France*
[b] *TotalEnergies, OneTech, R&D, CSTJF, Pau 64018, France*
[c] *Institut de Mécanique des Fluides de Toulouse, IMFT, Université de Toulouse, CNRS, 31400 Toulouse, France*
[d] *CERFACS, 42 avenue Gaspard Coriolis, 31057 Toulouse, France*
[e] *Greens Combustion Ltd, A31 Arena Business Centre, Holyrood Close, Poole, Dorset, BH17 7FJ, UK.*
[f] *CCA, Centro Combustione Ambiante, Via Milano, 70023 Gioia del Colle (BA), Italy*

Abstract

This study reports the results of an experimental campaign conducted in early 2025 to evaluate the Combustion Efficiency (CE) and Destruction Efficiency (DE) of pipe flares, which are the most widely used flaring devices in low-pressure gas networks at oil and gas facilities. The experiments investigated three flare diameters - 4", 8", and 14" - chosen to be representative of industrial-scale pipe flares (typically ranging from 10" to 60"), in contrast to sub-3" flares, which exhibit distinct combustion behaviors [1].

More than 100 measurements were performed under a wide range of operating conditions, including the presence or absence of a pilot flame and a windshield. The tests were conducted in a large combustion chamber where the flares were exposed to crosswind, with detailed monitoring of inlet parameters (flow rates, temperature, etc.) and downstream species concentrations (CO_2, CO, and CH_4).

This dataset is distinguished by its industrial relevance, high measurement quality, and strong repeatability. Consistent with previous studies [1, 2, 3, 4], the results confirm the Buoyancy Factor (BF) as the key parameter for characterizing flare performance and correlating CE/DE. The full dataset is publicly available [**?**].

Keywords: Combustion Efficiency, Pipe Flare, Experimental Campaign, Correlation, Buoyancy Factor

*Corresponding author: Ghislain Lartigue, ghislain.lartigue@gmail.fr

1. Motivation and objectives

Flaring devices are ubiquitous in industrial facilities for burning excess process gases, primarily for safety purposes. Two major types of flares are commonly used in the Oil and Gas industry: pipe flares and sonic flares. Pipe flares consist of a simple metal tube supplied with process gases from a low-pressure network. In contrast, sonic flares are often more complex and are typically connected to high-pressure gas networks to achieve sonic conditions at their nominal operating points. Sonic flares frequently incorporate vendor-specific technologies —such as variable slots, springs, or multi-arms— to enhance efficiency or operability. As a result, it is challenging to define a generic sonic flare, unlike pipe flares, which are inherently simple. In line with this observation, this article focuses exclusively on pipe flares.

Burning excess hydrocarbons rather than venting them is an effective way to reduce greenhouse gas (GHG) emissions, since the Global Warming Potential (GWP) of hydrocarbons is typically much higher than that of the carbon oxides produced during combustion [5]. The GWP quantifies how much heat a greenhouse gas traps in the atmosphere over a specified time horizon, relative to carbon dioxide. By definition, CO_2 has a GWP of 1, and the GWP of other gases is expressed as a multiple of this reference value.

It is important to note that GWP is defined on a per-mass basis. Consequently, for gas mixtures such as natural gas, which contains multiple hydrocarbons, the overall GWP must be calculated as a mass-weighted average of the GWPs of the individual components released to the atmosphere.

Table 1 summarizes the GWP values of the most common greenhouse gases [5, 6]. These values should be regarded as indicative, as their determination is complex and the reported figures have been revised several times over the past decades.

Gas	**GWP**
CO_2 (carbon dioxide)	1
CO (carbon monoxide)	0
CH_4 (methane)	27–30
C_2H_6 (ethane)	5.2–7.7
N_2O (nitrous oxide)	273

Table 1: Global Warming Potential (GWP) of common greenhouse gases over a 100-year time horizon [7, 8, 6]. Please note that the atmospheric lifetime of these molecules can vary by several orders of magnitude, thus their GWP depends on the time horizon considered.

As an example, Fig. 1 represents the GWP of the exhaust gases a flare fed by pure methane as a function of its conversion rate.

When conversion is zero, only methane is emitted, and the GWP is simply equal to $\mathrm{GWP}_{CH_4} = 30$. At 100% conversion, all CH_4 is oxidized to CO_2. Since GWP is defined on a mass basis rather than a volume basis, the resulting value is $(W_{CO_2}/W_{CH_4}) \times GWP_{CO_2} = 2.74$ when DE = 100%.

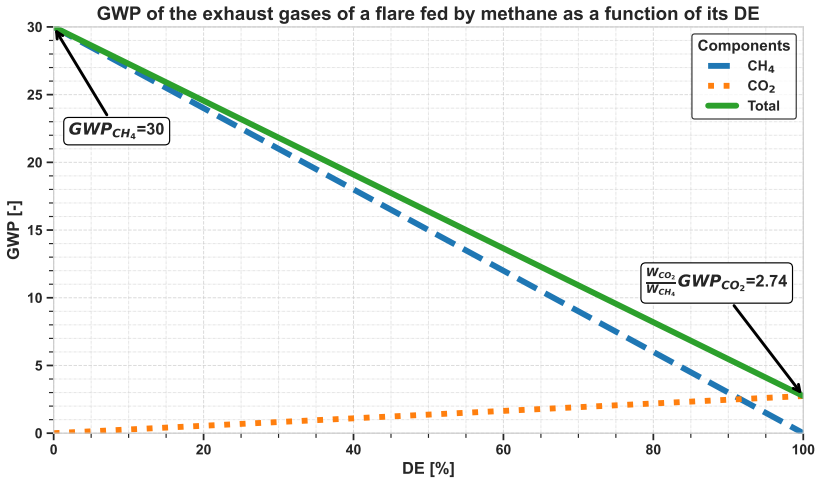

Figure 1: GWP of the exhaust of a flare fed by pure methane as a function of its destruction efficiency. The contribution from CO_2 is represented with orange dashes while the contribution from CH_4 is represented with blue dots. Their sum is represented with a solid green line.

A key observation is that even with a 90% conversion efficiency, the GWP of the emitted gas is still approximately 5 - nearly twice the value expected from complete combustion. This highlights that even modest improvements in flare combustion efficiency can yield substantial reductions in greenhouse gas emissions.

Knowing the real-time efficiency of flares is of primary importance for operating companies, both for safety reasons and for environmental reporting. In practice, however, most operators rely on a crude approximation, assuming a flare efficiency of 98% under all operating conditions. This rule of thumb [9, 10] is widely accepted and has even been incorporated into the OGMP2.0 standard[11, 12], despite its obvious and significant limitations.

The main reason is that the direct measurement of the efficiency of a flare in real conditions is extremely challenging: accessing the flare is usually difficult, the flame can be very long, its radiation very intense and any measurement must encompass the full plume to be relevant. The reader can refer to [13] for an excellent review of the various techniques that can be applied to measure flare efficiencies. Some direct techniques based on drones equipped with spectral analyzers are still in development [14] but with a limited operating range. Moreover these techniques are meant to be operated as spot/survey measurements, not for continuous monitoring. The other option to assess the efficiency of real equipments is to use indirect methods. A first approach is to perform imaging of the flame to assess its burnt gas composition and thus its efficiency: several systems based on this idea have been proposed recently [15, 16] but with a limited precision. Another long term goal is to propose an estimation of the efficiency via the use of a digital twin of the flare. This digital twin could be

obtained for example by performing some CFD simulations in various conditions. It must however be acknowledged that obtaining precisely the efficiency of a real-size flare seems out of reach of any CFD method for the time being: RANS approaches can hardly capture precisely the flame/turbulence interactions while LES struggles with the CPU cost associated to the resolution of the flame front [17, 18, 19, 20].

Finally, the most convincing approach to create a realistic digital model of the flare is to perform reduced-scale experiments and correlate the efficiency of the flare at upper scales by the use of relevant correlations.

This approach is not new and many experimental concepts to perform such measurements (rake, hood, wind tunnels, ...) were performed in the past decades and many correlations on conversion efficiencies were proposed based on those data [13]. However, our point of view is that they all suffer from some shortcomings that are detailed below:

1. the downscaled flare must still be representative of real-scale devices,
2. the physical behavior of the flare must be understood to propose relevant dimensionless number that will provide valid upscaling rules,
3. the measurements on the scaled-down flare must be performed with a high precision to propose a correlation with a sufficient accuracy.
4. the wind conditions must be perfectly controlled.

The first concern is already well documented [1]: it is now understood that the behavior of pipe flares with a diameter smaller than 3 inches is different from larger devices. Only medium-size flares must be considered to perform an upscaling and it is thus very difficult to assess the efficiency from lab scale experiments.

The second concern is less clear as many parameters can influence the flare behavior:

- flare: diameter, gas exit velocity (profile and turbulence), gas physical properties (density, viscosity, LHV)
- wind: wind velocity and turbulence level
- other: gravity intensity, flame characteristic speed and thickness

From these parameters, many dimensionless numbers can be built: Reynolds number, Froude number, Richardson number, Karlovitz number, velocity ratio, momentum ratio, buoyancy factor, ... Fortunately, many authors have already investigated this aspect [3, 4] and have already identified that the Buoyancy Factor (BF) seems to be the most promising parameter to characterize the flaring regime and to build a correlation between efficiency and operating conditions. It is also worth mentioning that the flare can include technological effects such as pilot flame or windshield that can not easily be incorporated in any dimensionless number

Regarding the third point, it is clear that the precision and accuracy of the measure must be extremely good to be of any relevance and to supersede the

well established 98% rule. The major difficulty is that measuring accurately unburnt hydrocarbons in very low concentrations (of the order of 100ppm) is not an easy task, even in laboratory conditions and it is even harder at semi-industrial scales.

Finally, the last point prevents to perform measurements in open air since the wind conditions can at best be monitored but in no way controlled.

Our objective is thus to overcome all these drawbacks by performing high-quality measurement of large scale pipe flares and to provide a correlation for conversion inefficiency based on our data. Three medium-size flares (4", 8" and 14") were investigated so that the correlation can be extrapolated safely to higher diameters. Moreover it enabled us to explore very low turndown ratios, similar to the ones observed in purge conditions on real assets (representing 80% of operating conditions) which are probably the most degraded conditions. Finally, the influences of pilot flame and windshield were also investigated on a limited set of operating conditions to gain some understanding on their influence on the combustion efficiency.

The remaining of the paper is organized as follows: section 2 presents the methodology and the experimental technique that was used to acquire our dataset, section 3 discusses the results with a first analysis and section 4 summarizes this study and briefly introduces the next steps.

All the experimental data presented in this paper are publicly available on the following web site **??**. This includes both the raw data of the tests (time series and values after steady state is reached for each operating point) as well as some images and videos of the flare for most of the measurement points.

2. Description of the method

2.1. Definitions of flare efficiencies

The classical indicators used to characterize the quality of the combustion in the flaring industry are the **Combustion Efficiency (CE)** and the **Destruction Efficiency (DE)**.

To understand their meaning, it is first important to recall the difference between complete and incomplete combustion.

Complete combustion of hydrocarbons is characterized by the fact that the only carbonated molecule in the burnt gases is CO_2. By opposition, incomplete combustion may leave unburned hydrocarbons in the combustion products. Moreover small amounts of CO can also be detected, serving as a marker of rapid dilution and quenching before the end of the combustion process in certain regions. As a consequence, the incomplete combustion of a stream of natural gas and a stream of air with molar flux $\dot{n}^{NG}$ and $\dot{n}^{Air}$ respectively into burnt gases (BG), can be represented schematically as:

$$\dot{n}^{NG} NG + \dot{n}^{Air} Air \rightarrow \dot{n}^{BG} BG \tag{1}$$

It is useful to introduce her for future use the **dilution rate** of the natural gas in the air:

$$\tau_m = \frac{\dot{m}^{Air}}{\dot{m}^{NG}} \quad \text{and} \quad \tau_n = \frac{\dot{n}^{Air}}{\dot{n}^{NG}} = \frac{W_{Air}}{W_{NG}} \tau_m \tag{2}$$

where W stand for molar mass, $\dot{m}$ indicates mass flow rates whereas $\dot{n}$ indicates molar flow rates. The dilution rate is directly linked to the global equivalence ratio of the setup.

The natural gas composition has not been specified yet but it is supposed that it is mainly composed of methane CH_4 plus a minority of other alkanes C_{2+} and traces of CO_2 and N_2. The presence of small amount of carbon dioxide and methane in the air can also been taken into account in this formula without any difficulty. Finally, it is supposed that the burnt gases are exclusively composed of the following species: N_2, O_2, H_2O, CO_2, CO and the alkanes present in the natural gas.

The composition of each constituents is summarized in Tab. 2.

Of course, thanks to atoms conservation, the composition of the burnt gases can be computed from the Natural Gas and Air molar fluxes and composition plus two hypothesis:

- any alkane molecule that reaches the Burnt Gases have not crossed the flame front. They are just unburnt hydrocarbons and are thus in the same proportion in the burnt gases than in the natural gas.
- the methane present in the Air is not affected by combustion. This is mostly true for high dilution rates as the ones considered here.

Species	Natural Gas	Air	Burnt Gases
N_2	$X_{N_2}^{NG}$	$X_{N_2}^{Air}$	$X_{N_2}^{BG}$
O_2	0	$X_{O_2}^{Air}$	$X_{O_2}^{BG}$
H_2O	0	0	$X_{H_2O}^{BG}$
CO_2	$X_{CO_2}^{NG}$	$X_{CO_2}^{Air}$	$X_{CO_2}^{BG}$
CO	0	0	X_{CO}^{BG}
CH_4	$X_{CH_4}^{NG}$	$X_{CH_4}^{Air}$	$X_{CH_4}^{BG}$
C_2H_6	$X_{C_2H_6}^{NG}$	0	$X_{C_2H_6}^{BG}$
C_3H_8	$X_{C_3H_8}^{NG}$	0	$X_{C_3H_8}^{BG}$
C_4H_{10}	$X_{C_4H_{10}}^{NG}$	0	$X_{C_4H_{10}}^{BG}$
C_5H_{12}	$X_{C_5H_{12}}^{NG}$	0	$X_{C_5H_{12}}^{BG}$
C_6H_{14}	$X_{C_6H_{14}}^{NG}$	0	$X_{C_6H_{14}}^{BG}$

Table 2: Notations used in this article for the composition of natural gas, air, and burnt gases.

More precisely, the incomplete combustion of a generic alkane present in the natural can be written as:

$$C_kH_{2k+2} + \gamma O_2 \longrightarrow \alpha C_kH_{2k+2} + (1-\alpha)\left[\beta k CO + (1-\beta)kCO_2 + (k+1)H_2O\right] \tag{3}$$

Atoms conservation implies that $\gamma = \frac{1}{2}(1-\alpha)\left[1+(3-\beta)k\right]$. The coefficient α represent the fraction of hydrocarbons that have not reacted at all while β represent the fraction of the remaining hydrocarbons that have reacted partially to form CO but not CO_2. Both must be in the interval $[0;1]$ and the reaction is complete only when $\alpha = \beta = 0$.

It is now possible to define:

- the **Destruction Efficiency (DE)** as *the fraction of carbon atoms initially present in the fuel as hydrocarbons that are still present under the form of hydrocarbon in the burnt gases* or equivalently as *the fraction of carbon atoms initially present in the fuel as hydrocarbons that has been converted to either CO or CO_2 in the burnt gases*, i.e. $DE = 1 - \alpha$.
- the **Combustion Efficiency (CE)** as *the fraction of carbon atoms initially present in the fuel as hydrocarbons that has been converted to CO_2 in the burnt gases*, i.e. $CE = (1-\alpha)(1-\beta)$.

The only difference between these two concepts is that the DE accounts for the presence of CO in the burnt gases whereas the CE does not. With these definitions, the relation $0 \leq CE \leq DE \leq 1$ is must hold. A CE or a DE close to one indicates a quasi-complete combustion. On the other hand, these indicators get closer to zero when the combustion becomes less and less efficient. Of course one can also define the **Combustion Inefficiency (CI)** and **Destruction Inefficiency (DI)** as $CI = 1 - CE$ and $DI = 1 - DE$.

It should be noted that, when it comes to estimate the GWP of the burnt gases in GHG reporting, the DE is probably a more relevant quantity compared

to CE, since it gives a direct evaluation of the remaining alkanes (with a high GWP) in the burnt gases.

These indicators can be expressed as:

$$CE = \frac{\dot{n}^{BG} X^{BG}_{CO_2} - \dot{n}^{Air} X^{Air}_{CO_2} - \dot{n}^{NG} X^{NG}_{CO_2}}{\dot{n}^{NG} X^{NG}_{C-alk}} \tag{4}$$

$$DE = \frac{\dot{n}^{BG} (X^{BG}_{CO} + X^{BG}_{CO_2}) - \dot{n}^{Air} X^{Air}_{CO_2} - \dot{n}^{NG} X^{NG}_{CO_2}}{\dot{n}^{NG} X^{NG}_{C-alk}} \tag{5}$$

where $\dot{n}^{NG} X^{NG}_{C-alk} = \dot{n}^{NG} \sum_k k X^{NG}_{C_k H_{2k+2}}$ represents the molar flux of carbon atoms *from the alkanes of the fuel.*

The Annex 7 presents in detail how to compute CE and DE from the available data with different levels of approximations. When no measure of mass flows are available or if they are considered as not reliable, the *Method 1* which relies exclusively on the gaz analyzer must be used. If the molar dilution rate of the natural gas in the air can be measured with a good precision from flow meters, the *Method 2* might be preferred.

Moreover, if one has access to the concentrations of CO, CO_2 and CH_4 in the burnt gases and if the dilution rate between natural gas and air is large, one can approximate CE and DE with the *Approximate Method 1* (M1A) as:

$$CE^{M1A} = \frac{X^{NG}_{CH_4} \Delta X^{BG}_{CO_2}}{X^{NG}_{CH_4} \left(\Delta X^{BG}_{CO} + \Delta X^{BG}_{CO_2}\right) + X^{NG}_{C-alk} \Delta X^{BG}_{CH_4}} \tag{6}$$

$$DE^{M1A} = \frac{X^{NG}_{CH_4} \left(\Delta X^{BG}_{CO} + \Delta X^{BG}_{CO_2}\right)}{X^{NG}_{CH_4} \left(\Delta X^{BG}_{CO} + \Delta X^{BG}_{CO_2}\right) + X^{NG}_{C-alk} \Delta X^{BG}_{CH_4}} \tag{7}$$

where $\Delta X^{BG}_k = X^{BG}_k - X^{Air}_k$ is the air-corrected measure of species k in the burnt gases. This formula generalizes the usual one which is only valid when $X^{NG}_{CH_4} = 1$ and $X^{NG}_{C-alk} = 1$, i.e. when the fuel is pure methane.

2.2. Experimental setup

All the results presented in this report were collected at the CCA facilities at Gioia Del Colle, Italy, during two distincts experimental campaigns: the first one from 14 to 17 January 2025 (4" and 8" flare) and the second on the 1st April 2025 (14" flare). The differences in the operating conditions between these two periods were sufficiently small to be ignored without impacting the analysis of the results.

The main novelty of these tests is that they were all conducted following the "Flare in a Box" concept which consists in enclosing the flare in a in a large combustion chamber (W=4m, H=4m, L=12m) that is then used as a wind tunnel as depicted in Fig. 3. The conversion efficiencies are finally retrieved by performing a gas composition analysis of the exhaust gases.

This concept is actually not totally new but has hardly ever been applied at this scale. For example, several authors performed similar testings but on much smaller scale [3, 4]. Because of the high dilution rate of the combustion

products, they also had to use a closed loop that recirculates the flow a large number of times to compensate the lack of precision of their analyzers. The main advantage of our method compared to other approaches like rakes and hoods is that we are guaranteed to have access to the full plume of the flare and not to miss any unburnt molecule. As a drawback, we can not access to local gas composition and we must cope with some possibly very long residence time in the furnace. This can be an issue to achieve temporal convergence in some situations, for example in low wind conditions when sweeping from high gas flow rates to low gas flow rates. To overcome this difficulty, the following procedure was followed for all operating points:

1. Set the wind velocity by varying the fan rotation speed, wait for a few minutes for stabilization
2. Set the natural gas flow rate: this is extremely fast (few seconds)
3. Wait for the convergence of all concentrations in the exhaust line. No quantitative criterion was used to assess this convergence: it was simply checked in real time thanks to the monitoring system via moving averages. Achieving convergence can take from 5 to 30 minutes according to the air flow rate. It is worth noting that the CE and DE usually converge to a steady state much faster than the concentrations.
4. Record data for 2 to 5 minutes to have meaningful statistics.

All the data have been acquired through a proprietary code developed on LabView which receives data from the plant Distributed Control System and the analyzers. This data is then recorded in the proprietary TDMS format (which can be read with a python module) and is also available as xls/csv files.

The combustion chamber is transformed into a wind tunnel by placing a so-called wind box at one of its end. The objective of this wind box is to create a lateral wind on the flare as it is expected to have a major impact on the conversion efficiency for low flaring rates. It is fed in air by two large fans which are controlled electrically: they were calibrated beforehand and it is expected that they can deliver flow rates ranging from 10t/h to 115t/h with an accuracy of 5% to 10%. The flare is located 2 meters downstream the wind box exit and the velocity profile at the flare tip is expected to be roughly flat. This has been demonstrated both by CFD and by hot wires measurements. The equivalent surface of the wind box has been measured to be $S_{WB} = 1.81m^2$. A maximum wind velocity of approximately 15m/s can be obtained at the flare tip and the turbulence intensity is supposed to be in the 5-10% range.

The flare is fed by natural gas from the city network. A gas composition analysis has been requested to the network operator a few weeks before the test campaign and is provided in Tab. 3. The physical properties of this natural gas are also summarized in Tab 4.

It is expected that this composition is rather stable over long period of times and thus no additional gas analysis was performed for the test campaign of April 2025. It is important to mention that no LHV variation has been tested during those campaigns: this was a deliberate choice since our primary interest resides

Component	**Formula**	X_k^{NG} **[% mol]**
Nitrogen	N_2	1.2686
Carbon Dioxide	CO_2	0.1916
Methane	CH_4	93.3316
Ethane	C_2H_6	3.1472
Propane	C_3H_8	1.2804
Butane	C_4H_{10}	0.5855
Pentane	C_5H_{12}	0.1809
Hexane	C_6H_{14}	0.0142
Total		100.0000

Table 3: Composition of the natural gas of Gioa del Colle gas network during the 2025 test campaign.

Global characteristics	**Unit**	**Value**
Molecular Weight	[kg/kmol]	17.406
Normal Density	[kg/Nm^3]	0.7766
High Heat Value	[kJ/kg$_{\mathrm{NG}}$]	53.661
Low Heat Value	[kJ/kg$_{\mathrm{NG}}$]	48.469
O_2 stech. Demand	[kg/kg$_{\mathrm{NG}}$]	3.851
CO_2 Exhaust Prod.	[kg/kg$_{\mathrm{NG}}$]	2.700
H_2O Exhaust Prod.	[kg/kg$_{\mathrm{NG}}$]	2.125

Table 4: Global characteristics of the natural gas of Gioa del Colle gas network during the January 2025 test campaign.

in E&P flares which mainly burn high-LHV gases. Based on the data presented above, the LHV ratio between the natural gas and pure methane is $\tau_{LHV} = 0.97$.

The flow rate of natural gas inside the flare $\dot{n}^{NG,f}$ is controlled by a flow meter which is calibrated to operate from 1 g/s to 60 g/s. Table 5 summarizes for each flare the turndown ratios associated to the minimum and maximum natural gas flow rates during the tests. This ratio between the flow rate at design point and the actual flow rate is of primary importance to validate the relevance of the tests. A statistical analysis of the turndown ratios of several flares operated by TotalEnergies confirmed that this was spanning most of the operating conditions of real flares, i.e. from purge rate to a significant fraction of the design point.

An additional (but very low) flow rate of natural gas $\dot{n}^{NG,p}$ can also be send to the pilot when it is used to enhance the flare stability. The mass flow rate of Natural Gas in the pilot was varied slightly during the test campaign: it was set to the lowest possible values in the 4"-flare and 14"-flare campaigns, in contrast with the initial 8"-flare campaign where it was set to a relatively high value with respect to the flare size. More specifically, it was set to:

- $\dot{m}_{4"}^{NG,p} = 0.3$ g/s for the 4 inches flare,
- $\dot{m}_{8"}^{NG,p} = 1.0$ g/s for the 8 inches flare,

Flare diameter	4”	8”	14”
Design NG flow rate [g/s]	1’250	5’000	15’000
Minimum tested NG flow rate [g/s]	1	1	3
Maximum tested NG flow rate [g/s]	20	40	60
Turndown ratio at Minimum tested	1’250	5’000	5’000
Turndown ratio at Maximum tested	60	125	250

Table 5: Turndown ratios for the three flares.

- $\dot{m}_{14"}^{NG,p} = 0.5$ g/s for the 14 inches flare,

Naturally, the natural gas flowing through the pilot flame was taken into account during the computation of the flare efficiency. However, it was supposed that the main flame and the pilot flame have the same efficiency: this is not really accurate since the efficiency of the pilot is probably very close to 100% in most situations. Anyway, this should only have a very limited influence on the results except for very low flare flow rates.

Finally, the combustion products are convected downstream the furnace and collected through an exhaust system. A gas sampler is inserted in this exhaust system, far from the furnace exit and after several turns: this guarantees that the mixture is nearly homogeneous in the section where the sample is collected and that the precise sampling point is irrelevant. This sample then flows to a gas treatment station (filtering and water removal) and to an online Horiba VA-5111 analyzer that provide real-time values (1Hz) for the volume fraction of CO_2, CO and CH_4. Please note that the dilution rate is so high in all operating conditions that there is no need to apply a correction to accommodate for the water removal. This analyzer was calibrated before the tests with known composition samples (see certificate in Section 8). The modules in the analyzer were selected to obtain the best precision in the ranges indicated in Tab. 6 that were precomputed to accommodate with all the operating conditions and particularly with the dilution rate that can span several orders of magnitude.

Molecule	Lower Scale	Higher Scale	Precision
CO_2	1’000 [ppmv]	10’000 [ppmv]	1% of the Full Scale
CO	50 [ppmv]	500 [ppmv]	1% of the Full Scale
CH_4	100 [ppmv]	1’000 [ppmv]	1% of the Full Scale

Table 6: The Horiba VA-5111 has two predefined ranges for each species.

This furnace benefits from several optical accesses on both lateral walls: five video streams of the flare with different angles, fields of view, exposures, focal, aperture, ... were acquired during the January 2025 campaign as described more precisely in section 2.3.

Our three LP flaring systems (4", 8" and 14", see Fig.2a, Fig.2b and Fig.2c) were provided by Greens Combustion Limited. Each consists of a vertical tube which is fed by the bottom with Natural Gas and augmented with two additional components to mimic more closely real flares:

1. The pilot burner with an exit diameter of 36.2mm provides an ignition flame to the main flare tip. This pilot can be remotely ignited with a high voltage ignition electrode. This flame is obtained by premixing a small amount of natural gas with air in a Venturi system. This pilot Venturi design inspirates 60-80% of stoichiometric air with the balance of the required air for complete combustion being inspirated as the gas/air mixture exits the nozzle. This is therefore semi-premixed flame. This pilot flame can be switched on and off on demand but the tube is always mounted on the flare.
2. A windshield which consists of vertical metal bars located around the tip of the flare. Its primary purpose is to prevent flame pull down onto the body of the flare in high lateral wind conditions and low flare gas exit velocity. However it can provide enhanced flame stability by providing a low-speed recirculation zone near the flare body. The flare tips also come with two lateral flame holders which are bended metal bars attached to the top of the pipe, near the pilot. The purpose of these is typically to anchor the flame at higher flare gas exit velocities by creating a turbulent zone near the fare pilots. This windshield (abbreviated as WS) can be removed easily to test its influence on the conversion efficiency.

2.3. Imaging system

A secondary objective of this campaign was to collect a series of flame images based on various input parameters (gas flow rate and wind speed), labeled with the measured CE/DE. This database will subsequently be used to develop a model that can predict the CE/DE from either a single or a series of flame image. To this end, five cameras (C_1 to C_5) were used to capture the details of the flames in the combustion chamber during the test as depicted in Fig. 3:

- 2 on the left side with 2 different focal lens (C_1 - C_2)
- 1 on the right side (C_3)
- 1 inside for a bottom view (C_4)
- 1 inside for a top view (C_5)

The images were recorded at 20 frames per second (fps) for 2 minutes each. This provides 2'400 high-definitions images for each operating condition that can be used to perform some statistical analysis or model training. The amount of image data collected from the five cameras is more than $2.6TB$ of *tif* compressed image data. The campaign data are listed in table 7. A small subset of these images (instantaneous and average) are directly available in [**?**] and the remaining is available upon request.

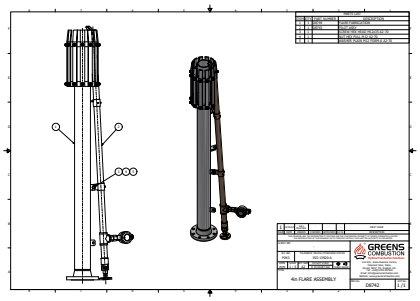

(a) 4” flare

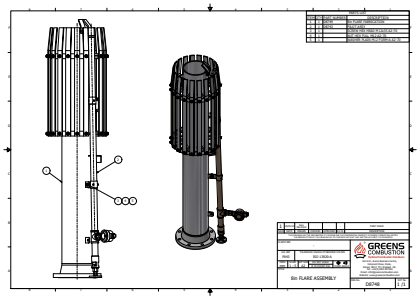

(b) 8” flare

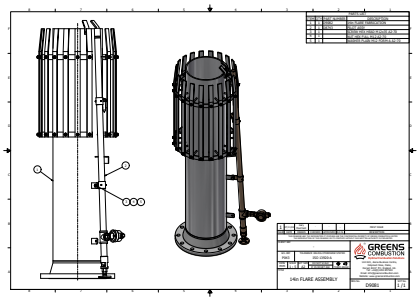

(c) 14” flare

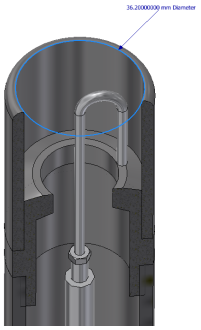

(d) Pilot system

Figure 2: Details on the flares and pilot

Feature	Quantity
Operating Conditions	104
Video frame per second	20
Duration	120s / 2’400 images
Images per camera	197×10^3
Total images	628×10^3
Total recording time	2h45
Amount of data	2.6 TB

Table 7: Dataset amount of data

Figure 4 shows an overview of the appearance of the flames for the 8” and 4” flares (with pilot on and wind shield on) taken by the camera C_3 for all the available operating conditions, i.e. air and gas flow rates. In this images, the air flows from the left to the right and the thumbnail was chosen randomly in the corresponding dataset.

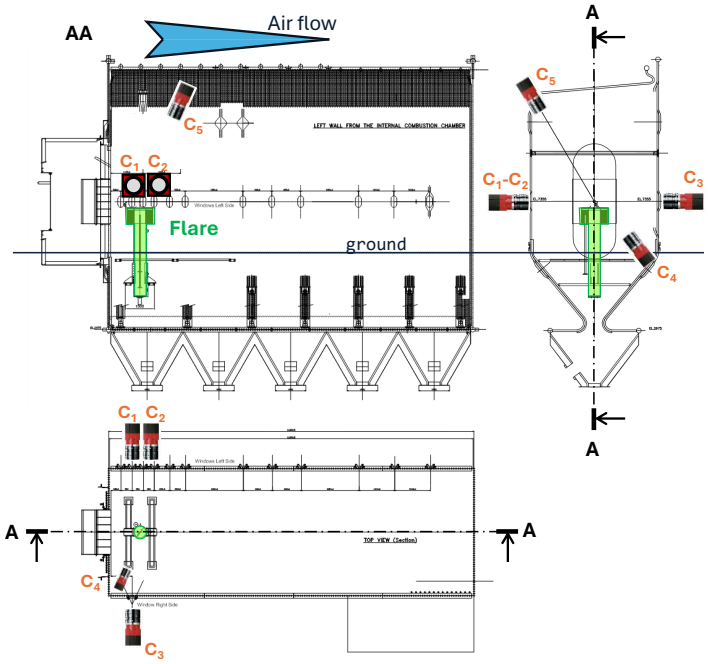

Figure 3: CCA combustion chamber with camera locations (C_1 to C_5)

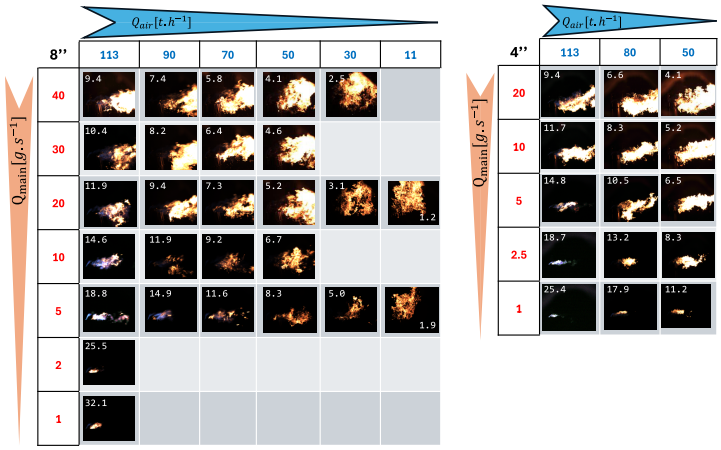

Figure 4: Overview of the images of the 8" and 4" flares with theirs respective buoyancy factors taken by the camera C_3

3. Results and Analysis

This section first describes the procedure that was used to evaluate the precision and repeatability of the setup followed by the results obtained with the three flares.

All measurement points are labeled with a three-digit ID to allow a one-to-one mapping between the data reported here and the raw data provided as supplementary material.

The final subsection proposes correlations for the CE and DE based on these results.

3.1. Reference atmospheric values

The first measurement (ID=001) was performed by flowing pure air through the combustion chamber and was solely intended to determine the CH_4 and CO_2 concentrations in the ambient air during the test campaign. The measured volume fractions were $X^{Air}_{CO_2} = 441$ ppm and $X^{Air}_{CH_4} = 3.0$ ppm.

These values are fully consistent with measurements performed at the Mauna Loa Observatory, which serves as a worldwide reference (CO_2 trends and CH_4 trends) [21, 22].

It should be noted that the CH_4 concentration is very low and comparable to the precision of the Horiba VA-5111 analyzer. Nevertheless, this concentration consistently remained between 2.9 ppm and 3.5 ppm throughout the entire calibration procedure (1h30), demonstrating the stability and reliability of the analyzer. Moreover, similar measurements were performed informally each morning during the five-day campaign and the results were systematically consistent with these reference values.

3.2. Verification of the air flow rate metering system

The precision of both the CO_2 flow meter and the gas analyzer is of the order of a few percent in the operating regime considered. By contrast, the measurement of the air flow rate is expected to be less precise for several reasons, as detailed below. The control parameter for the air flow rate is the voltage applied to the fans, and the actual flow rate is obtained through a static correlation. However, the accuracy of this correlation can be affected by several environmental factors: the chamber pressure is regulated via shutters that may not always be positioned identically, the air density can vary by a few percent depending on weather conditions, the chamber is not perfectly airtight, the flow of natural gas through the flare increases the pressure chamber, ...

The objective of this calibration campaign is therefore to quantify the precision of the air flow rate measurement by computing it from the CO_2 flow meter and gas analyzer data. To this end, pure CO_2 was injected into the chamber via the flare while lateral wind was induced by the fans and the resulting concentration in the exhaust gases was then measured. Table 8 summarizes the measurements performed during the calibration campaign.

ID units	$\dot{m}^{Air}$ [t/h]	$\dot{m}^{CO_2}$ [g/s]	$X^{BG}_{CH_4}$ [ppm]	$X^{BG}_{CO_2}$ [ppm]
001	113.8	0.0	3.0	441
002	113.8	20.1	3.0	858
003	113.8	50.1	3.0	1414
004	100.1	50.1	3.0	1554
005	80.7	50.1	3.0	1795
006	60.5	50.1	3.0	2230
007	40.2	50.1	3.0	3080
008	20.4	50.1	3.0	5520
009	14.2	50.1	3.0	7450

Table 8: Results of the calibration tests without combustion.

The air flow rate can then be estimated via a simple mass balance on CO_2:

$$\dot{m}^{Air,\mathrm{GA}} = \frac{W_{air}}{W_{CO_2}} \cdot \frac{\dot{m}^{CO_2}}{X_{CO_2} - X^{air}_{CO_2}}, \tag{8}$$

and compared to the reference value estimated from the flow meter, $\dot{m}^{Air,\mathrm{FM}}$ where GA stands for Gas Analyzer while FM stands for Flow Meter.

These results are presented graphically in Fig. 5.

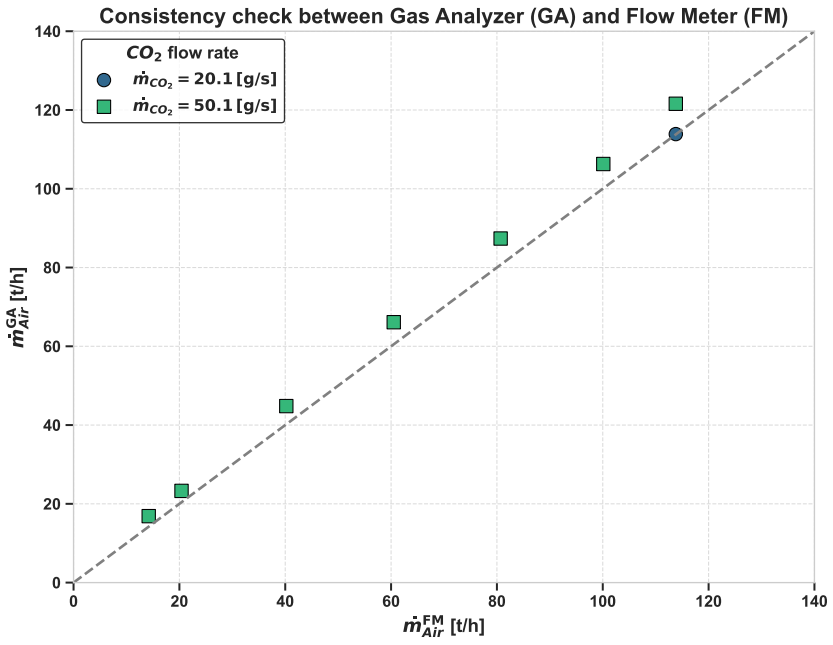

Figure 5: Comparison of the air flow rates computed from the flow meter and the gas analyzer. The quasi-linearity indicates a good consistency between the two independent measures.

The main observation is that the correlation between $\dot{m}^{Air,\mathrm{GA}}$ and $\dot{m}^{Air,\mathrm{FM}}$

is good and a linear fit between those data shows that:

$$\dot{m}^{Air,\mathrm{GA}} = \alpha.\dot{m}^{Air,\mathrm{FM}} + \beta \tag{9}$$

with $\alpha = 1.0515$, $\beta = 2.28$ t/h and with a coefficient of determination $R^2 = 0.99983$. This indicates a very good linearity between both approaches with a systematic error of the order of 5% between both methods for high air flow rates. Consequently the air flow rate $\dot{m}^{Air,\mathrm{FM}}$ will be used in the rest of this article without any additional correction and an uncertainty of 5% will be retained when needed.

3.3. Repeatability verification

Another important quality indicator of the setup is its ability to reproduce the same measurements with the lowest possible dispersion in the results. Table 9 presents the results obtained on 3 sets of identical conditions. It should be noticed that most of these measurements are separated by one day, except points 025 and 028 which are only half an our apart but two intermediate operating conditions were performed during this interval.

It appears that the repeatability is excellent: the deviation on all the concentrations is of the order of 3% in the worst cases.

ID	$\dot{m}^{Air}$	$\dot{m}^{NG,f}$	$\dot{m}^{NG,p}$	Pilot	$X^{BG}_{CH_4}$	$X^{BG}_{CO_2}$	X^{BG}_{CO}
units	[t/h]	[g/s]	[g/s]	-	[ppm]	[ppm]	[ppm]
010	113.7	40.0	1.0	ON	90.3	2724	22.0
025	113.7	40.0	1.0	ON	92.8	2652	22.0
028	113.7	40.0	1.0	ON	92.1	2697	22.1
022	113.7	40.0	0.0	OFF	138.0	2585	29.0
026	113.7	40.0	0.0	OFF	138.4	2557	28.6
023	113.7	40.0	1.0	OFF	151.7	2651	29.7
027	113.7	40.0	1.0	OFF	152.9	2605	29.7

Table 9: Evaluation of the repeatability of our setup for 3 different operating conditions.

3.4. Results and Analysis

All the results are gathered in Tab 11 to Tab. 17 in Annex 6 and are represented graphically in Fig. 6 to Fig. 8.

Several comments can be made on these figures:

- Each flare has been given its own color code: blue for 4", red for 8" and green for 14"
- The maximum velocity that can be reached by the gas at the exit of the flare is lower for large flares due to the increase of the exit surface. The choice has however been made to keep a common scale on the horizontal axis for a better comparison.

- The hue scale is in one to one correspondence with the wind speed (lighter for low velocity, darker for high velocity) is kept constant across all graphs to ease the visual interpretation.
- The solid lines correspond to CE/DE computed with the Exact Method 1 (M1E) while Exact Method 2 (M2E) is represented with dotted lines.
- The efficiencies obtained by both methods are similar except for low gas velocity. The discrepancy in this region increases when the wind velocity increases.
- The CE and the DE are behaves similarly. The DE is always lower as expected.
- The first global trend is that the CI increases when wind speed increases. This effect is not marginal as reported previously.
- The second global trend is that the CI increases when gas speed decreases.
- However, when the flare is large enough and it is equipped with a windshield it is observed that the efficiency can increase slightly for very low gas flow rates: this is probably due to the fact that the flame sits inside the flare tube where it can burn with a better efficiency in a more premixed mode.
- It is confirmed that the pilot and the windshield have a positive influence on the efficiency
- In the worst configuration (pilot off and wind shield off) the flame was blown off for high wind velocity and low gas flow rates (not directly visible on the figures).
- Such extinctions never occur in any other cases.

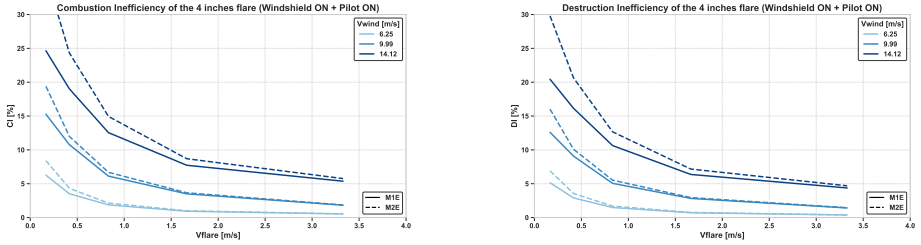

(a) CI - wind shield ON - pilot ON

(b) CI - wind shield ON - pilot ON

Figure 6: Combustion Inefficiency (left) and Destruction Inefficiency (right) of the 4 inches flare as a function of the flare exit velocity and indexed by the wind velocity. M1E: Method 1 Exact. M2E: Method 2 Exact.

It is however difficult to find a direct correlation between efficiency, wind velocity and gas velocity from these figures. A basic physical analysis shows

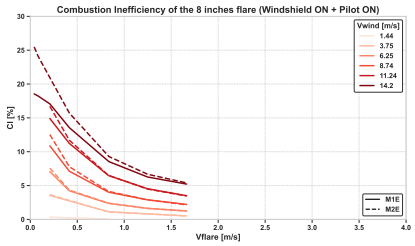

(a) CI - wind shield ON - pilot ON

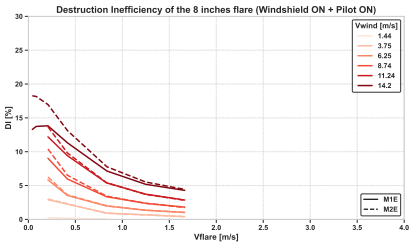

(b) DI - wind shield ON - pilot ON

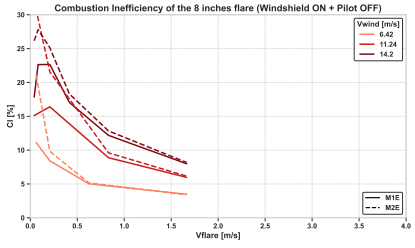

(c) CI - wind shield ON - pilot OFF

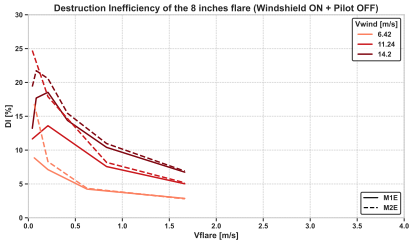

(d) DI - wind shield ON - pilot OFF

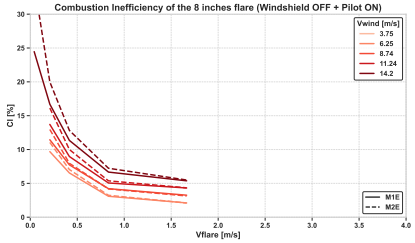

(e) CI - wind shield OFF - pilot ON

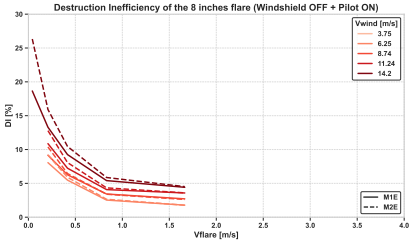

(f) DI - wind shield OFF - pilot ON

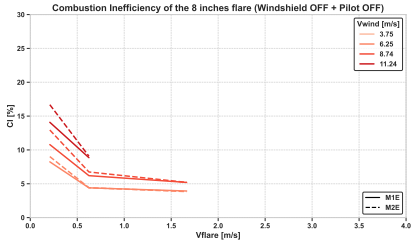

(g) CI - wind shield OFF - pilot OFF

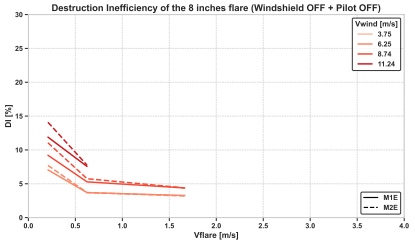

(h) DI - wind shield OFF - pilot OFF

Figure 7: Combustion Inefficiency (left) and Destruction Inefficiency (right) of the 8 inches flare as a function of the flare exit velocity and indexed by the wind velocity. M1E: Method 1 Exact. M2E: Method 2 Exact.

that the CE and the DE primarily depend on the mixing between the fuel and the air. Several mechanisms contribute to the mixing process, including Kelvin-

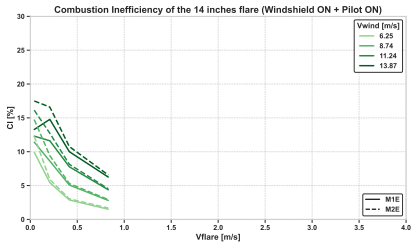

(a) CI - wind shield ON - pilot ON

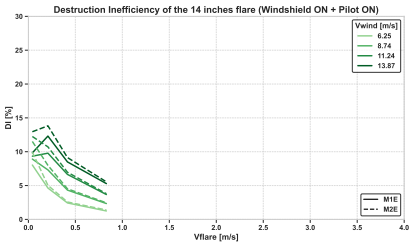

(b) DI - wind shield ON - pilot ON

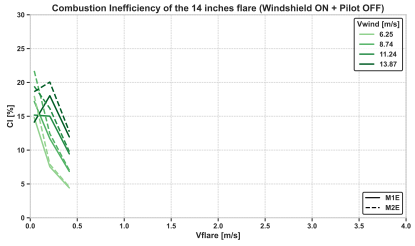

(c) CI - wind shield ON - pilot OFF

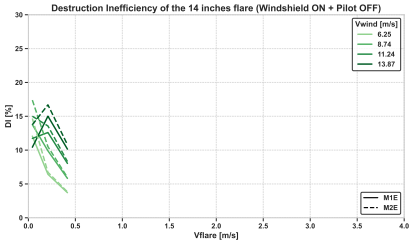

(d) DI - wind shield ON - pilot OFF

Figure 8: Combustion Inefficiency (left) and Destruction Inefficiency (right) of the 14 inches flare as a function of the flare exit velocity and indexed by the wind velocity. M1E: Method 1 Exact. M2E: Method 2 Exact.

Helmholtz instabilities in the shear layer, outer turbulence, inner turbulence, buoyancy, ...

Johnson et al. [3] have already identified the **Buoyancy Factor (BF)** as the relevant parameter for correlating combustion efficiency:

$$\mathrm{BF} = \frac{V_{\mathrm{wind}}}{\left(g D_{\mathrm{flare}} V_{\mathrm{flare}}\right)^{1/3}} \tag{10}$$

This will be confirmed by the analysis below.

The main reason is that the presence of unburnt hydrocarbons in the exhaust gases can only be understood as a *no combustion* process rather than an *incomplete combustion* process. Indeed, in the last situation, no alkane can survive past the flame front and only CO would be produced in large quantity if quenching would occur. The presence of unburnt hydrocarbons is thus a marker of leakage of the fuel through holes in the flame. Indeed, as soon as the flame is not attached to the flare tip, such holes can occur and this creates a path for the fuel which can escape far from the flame, get diluted with air and becomes non flammable (below the Lean Flammability Limit). When the wind velocity increases, this phenomenon is amplified and the conversion rate of the flame decreases. This ability of the fuel to escape far from the flame is thus determined by basic fluid dynamics in the vicinity of the flare tip where the buoyancy of the methane plays a major role rather than combustion-related properties. This

explains why the BF is a relevant parameter to correlate the DI with in these regimes.

This observation led Johnson and Kostiuk from University of Alberta (UoA) [3, 23, 24] to estimate the Combustion Inefficiency of a flare as:

$$CI_{UoA} = A_{UoA} \cdot \exp\left(B_{UoA} \cdot BF\right) \cdot \tau_{LHV}^{3} \tag{11}$$

with $A_{UoA} = 0.001066$ and $B_{UoA} = 0.317$ and $\tau_{LHV} = \frac{LHV_{CH4}}{LHV_{Fuel}}$. A similar analysis was thus performed on the dataset presented above to confirm this correlation and the results are presented in Fig. 9. Those figures only present the results of the flares in their optimal setup (pilot on and wind shield on).

On this figures, the correlation from Eq. 11 is indicated with a thick black line. It appears that this correlation underestimates both the CI and the DI in the $0 < BF < 15$ range. This is not really surprising since this correlation was obtained on flares with a small diameter (1 cm to 5 cm). This is clearly below the 3" limit and the scaling of this law to larger flare is questionable. Moreover, due to the limited size of their setup, the maximum reported BF for natural gas was 15. The proposed correlation behaves correctly up to this point but gives absurd results as soon as BF increases since the CI increases monotonically with BF and becomes larger than 1 for $BF > 21.6$ This is in clear contrast with the results of the current campaign which indicates that larger flares reaches a plateau when the Buoyancy Factor continues to increase. As already discussed, this is probably linked to the fact that when $BF > 15$ the flame sits inside the flare rather than outside and this changes fundamentally the hydrocarbon leakage mechanism.

To accommodate with this remark, the following new model for the Inefficiency is proposed:

$$I_{\mathrm{TTE}} = A \times \frac{1}{2}\left[1 + \tanh\left(\frac{BF - BF_0}{\Delta}\right)\right] \tag{12}$$

Equation 12 is valid bot for CI and DI with the numerical values indicated in Tab. 10.

coefficient	A	BF_0	Δ
CI	0.18	11.5	5.5
DI	0.13	11.1	5.5

Table 10: Numerical values of the coefficients that must be used in Eq. 12 for both the CI and the DI

These fits are also indicated with a thick magenta line in the Fig. 9. It seems to be very accurate when $BF < 15$. Even if still coherent, the result is less precise above this limit since the BF might not be the best parameter to fit CI/DI in this new situation where the flame behavior changes dramatically. This is indicated with a shaded gray area in the figures.

A statistical analysis of real flares operated by TotalEnergies have however shown that a Buoyancy Factor above 15 corresponds to exceptional situations.

The same analysis was performed for degraded conditions (pilot and/or wind shield off) as shown in Fig. 10 and Fig. 11. It clearly appears that the correlation presented in Eq. 12 remains valid even if the numerical values must be adapted to cope with the efficiency degradation. This has not been done in the present study: the coefficients are thus only valid for flares in their optimal setup.

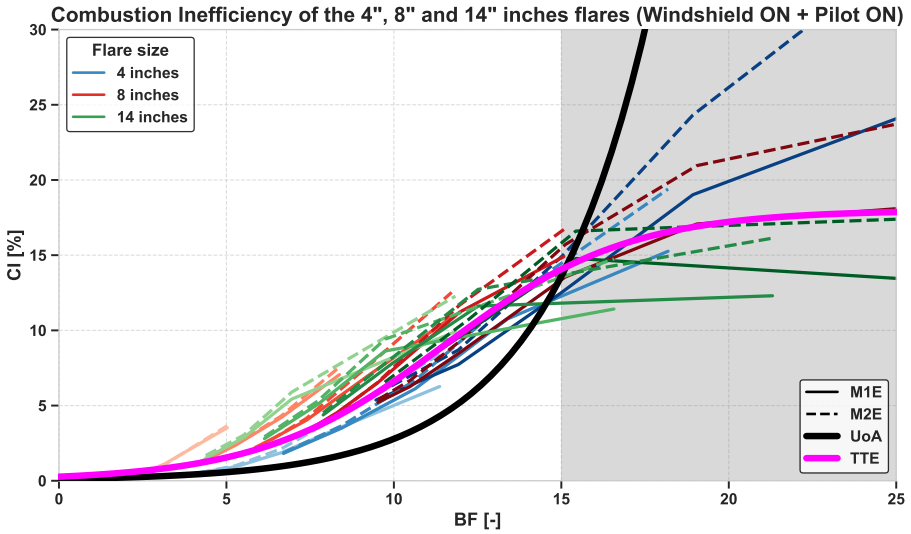

(a) Combustion Inefficiency

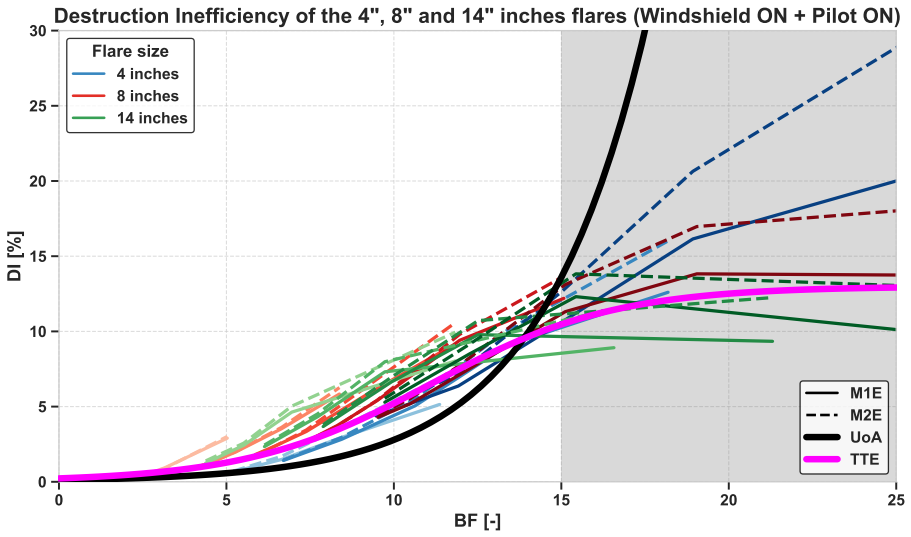

(b) Destruction Inefficiency

Figure 9: Combustion Inefficiency (9a) and Destruction Inefficiency (9b) of the three tested flares with Pilot ON and wind shield ON as a function of the Buoyancy Factor. M1E: Method 1 Exact. M2E: Method 2 Exact. The correlation from the University of Alberta (UoA) is indicated with a thick black line. The newly proposed correlation (TTE) is indicated with a thick magenta line.

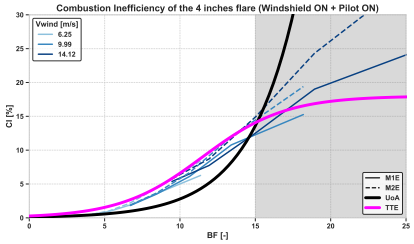

(a) 4” flare - wind shield ON - pilot ON

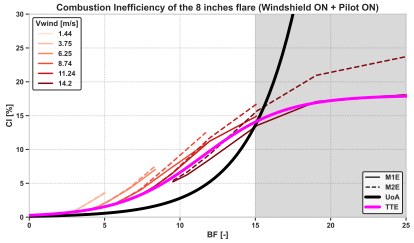

(b) 8” flare - wind shield ON - pilot ON

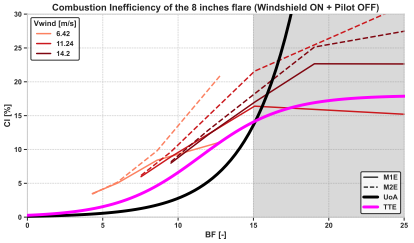

(c) 8” flare - wind shield ON - pilot OFF

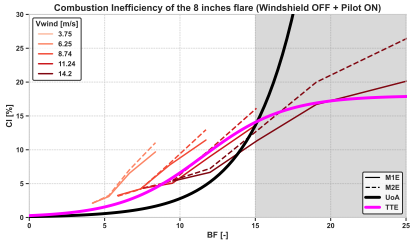

(d) 8” flare - wind shield OFF - pilot ON

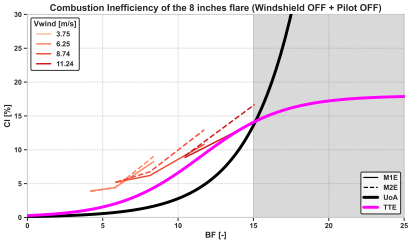

(e) 8” flare - wind shield OFF - pilot OFF

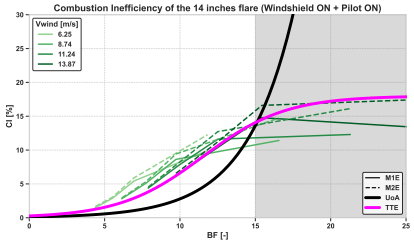

(f) 14” flare - wind shield ON - pilot ON

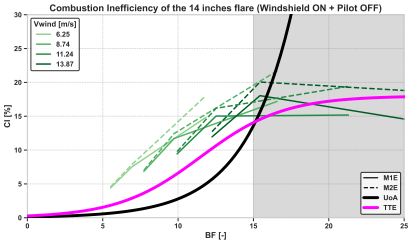

(g) 14” flare - wind shield ON - pilot OFF

Figure 10: Individual Combustion Inefficiency of the 4”, 8” and 14” flares in different configurations as a function of the Buoyancy Factor. M1E: Method 1 Exact. M2E: Method 2 Exact. The correlation from the University of Alberta (UoA) is indicated with a thick black line. The newly proposed correlation (TTE) is indicated with a thick magenta line.

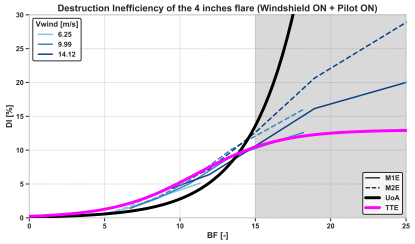

(a) 4” flare - wind shield ON - pilot ON

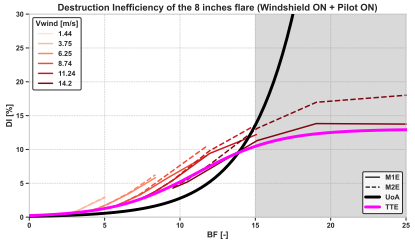

(b) 8” flare - wind shield ON - pilot ON

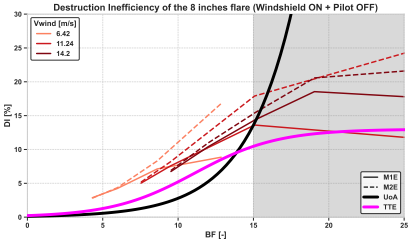

(c) 8” flare - wind shield ON - pilot OFF

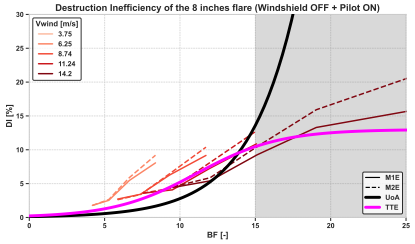

(d) 8” flare - wind shield OFF - pilot ON

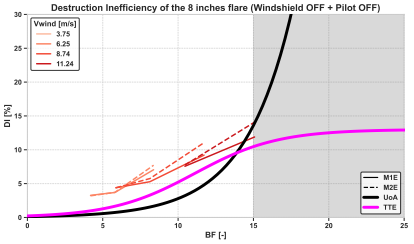

(e) 8” flare - wind shield OFF - pilot OFF

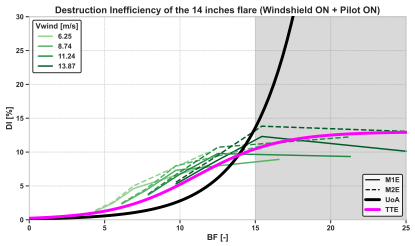

(f) 14” flare - wind shield ON - pilot ON

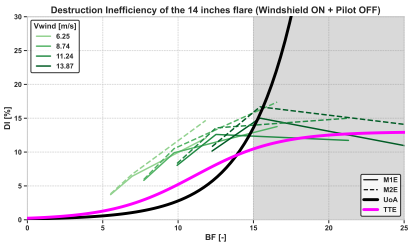

(g) 14” flare - wind shield ON - pilot OFF

Figure 11: Individual Destruction Inefficiency of the 4”, 8” and 14” flares in different configurations as a function of the Buoyancy Factor. M1E: Method 1 Exact. M2E: Method 2 Exact. The correlation from the University of Alberta (UoA) is indicated with a thick black line. The newly proposed correlation (TTE) is indicated with a thick magenta line.

4. Conclusion and perspectives

A high-quality dataset on the combustion efficiency of pipe flares has been presented. This work is unprecedented in several respects:

- the size of the flares considered which is comparable to real industrial flares,
- the extended range of operating conditions,
- the investigation of stabilization devices such as pilot flames and wind shields,
- and the original experimental setup used to acquire the data.

Combustion Efficiency and Destruction Efficiency were systematically and carefully evaluated under all operating conditions using two independent methods. Based on these results, a new correlation is proposed that outperforms the one of Johnson and Kostiuk [3], which is likely only valid for flares with smaller diameters.

Although the findings are very encouraging, this study should be complemented by datasets obtained with lower-LHV gases or with steam- or air-assisted flares. Finally, it must be emphasized that the proposed correlation applies only to pipe flares: high-pressure sonic flares are fundamentally different, and the correlation will likely fail if applied to them directly.

5. Authors contribution

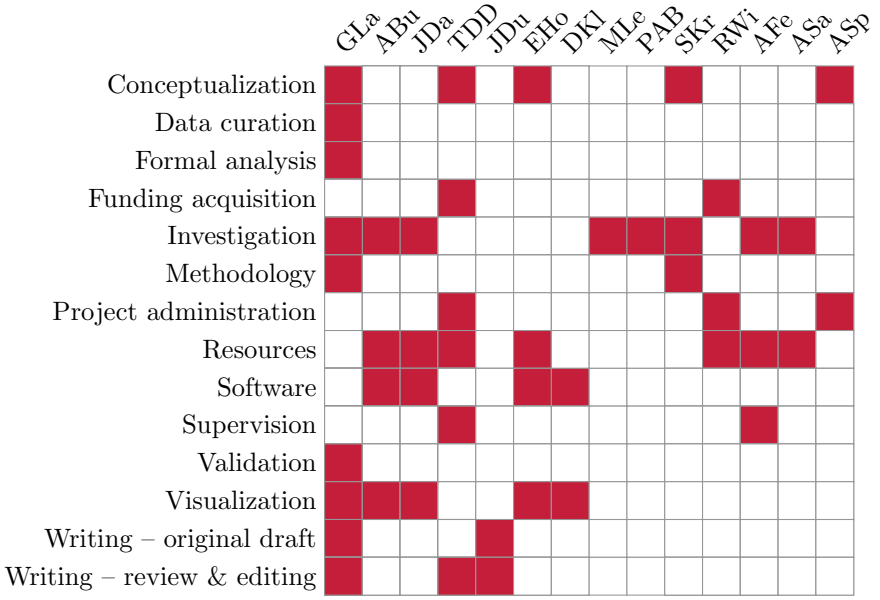

References

[1] Peter Gogolek. Explaining the 'three inch rule': Why model flares don't match full-scale. In *FRC 2022 Industrial Combustion Symposium*, 1 Haanel Drive, Ottawa, ON, Canada, K1A 1M1, 2022. NRCan/Canmet ENERGY-Ottawa.

[2] John H. Pohl, R. Payne, and J. Lee. Evaluation of the efficiency of industrial flares: Test results. Technical Report EPA/600-S2-84-095, U.S. Environmental Protection Agency, Industrial Environmental Research Laboratory, 1984.

[3] M.R Johnson and L.W Kostiuk. Efficiencies of low-momentum jet diffusion flames in crosswinds. *Combustion and Flame*, 123(1):189–200, 2000.

[4] D.C. Burtt, D.J. Corbin, J.R. Armitage, B.M. Crosland, A.M. Jefferson, G.A. Kopp, L.W. Kostiuk, and M.R. Johnson. A methodology for quantifying combustion efficiencies and species emission rates of flares subjected to crosswind. *Journal of the Energy Institute*, 2022.

[5] Wikipedia. Global warming potential. `https://en.wikipedia.org/wiki/Global_warming_potential`, 2025.

[6] Intergovernmental Panel on Climate Change (IPCC). Climate change 2021: The physical science basis. contribution of working group i to the sixth assessment report of the ipcc, 2021. Table 7.SM.7 for detailed GWP values.

[7] G. Myhre, D. Shindell, F.-M. Bréon, W. Collins, J. Fuglestvedt, J. Huang, D. Koch, J.-F. Lamarque, D. Lee, B. Mendoza, T. Nakajima, A. Robock, G. Stephens, T. Takemura, and H. Zhang. Anthropogenic and natural radiative forcing. *Nature Geoscience*, 6:924–937, 2013.

[8] Intergovernmental Panel on Climate Change (IPCC). Climate change 2013: The physical science basis. contribution of working group i to the fifth assessment report of the ipcc, 2013. Table 8.A.1 for GWP values.

[9] John L. Sorrels, Jeff Coburn, Kevin Bradley, and David Randall. Chapter 1 – flares. Air pollution control cost manual, section 3.2: Voc destruction controls, U.S. Environmental Protection Agency, Office of Air Quality Planning and Standards, Research Triangle Park, NC, August 2019.

[10] D. T. Allen and V. M. Torres. Tceq 2010 flare study final report. Technical report, Texas Commission on Environmental Quality (TCEQ), 2011. PGA No. 582-8-862-45-FY09-04 with supplemental support from TCEQ Grant No. 582-10-94300.

[11] Alexandrina Platonova-Oquab. 2025 global gas flaring tracker report. Technical report, World Bank Group, Global Flaring and Methane Reduction (GFMR) Partnership, July 2025. Published July 18, 2025.

[12] Elizabeth McGurk. Ogmp 2.0: Comparing direct measurement requirements with the revised epa subpart w rule, 2024.

[13] Kyle J. Daun and Jennifer P. Spinti. Techniques for measuring flare combustion efficiency and destruction removal efficiency: A review. *Progress in Energy and Combustion Science*, 110:101235, 2025.

[14] J.-L. Bonne, L. Donnat, G. Albora, J. Burgalat, N. Chauvin, D. Combaz, J. Cousin, T. Decarpenterie, O. Duclaux, N. Dumelié, N. Galas, C. Juery, F. Parent, F. Pineau, A. Maunoury, O. Ventre, M.-F. Bénassy, and L. Joly. A measurement system for co_2 and ch_4 emissions quantification of industrial sites using a new in situ concentration sensor operated on board uncrewed aircraft vehicles. *Atmospheric Measurement Techniques*, 17(14):4471–4491, 2024.

[15] Y. Zeng, J. Morris, A. Sanders, S. Mutyala, and C. Zeng. Methods to determine response factors for infrared gas imagers used as quantitative measurement devices. *Journal of the Air & Waste Management Association*, 67(11):1180–1191, November 2017.

[16] Paule Lapeyre, Rodrigo Brenner Miguel, Michael Christopher Nagorski, Jean-Philippe Gagnon, Martin Chamberland, Caroline Turcotte, and Kyle J. Daun. Quantifying flare combustion efficiency using an imaging fourier transform spectrometer. *Journal of the Air & Waste Management Association*, 74(5):319–334, 2024.

[17] M. Cremer, D. Wang, M. McGurn, and J. Thornock. Leveraging the uintah computational framework for commercial simulation of industrial flares. Paper presented at the American Flame Research Committee (AFRC) Conference, 2018; available as PDF via University of Utah Marriott Library Digital Collections, September 2018. AFRC 2018 conference paper; type = event; format: PDF; abstract available online.

[18] Anchal Jatale, Philip J. Smith, Jeremy N. Thornock, Sean T. Smith, and Michal Hradisky. A Validation of Flare Combustion Efficiency Predictions From Large Eddy Simulations. 1(2):021001.

[19] Jeremy Thornock, Philip Smith, and Allan K. Chambers. Les simulations of sour gas flares in western canada. Report, American Flame Research Committee (AFRC), 2009. Numerical simulation development using an ARCHES LES model (with chemistry and radiation) for sour gas flare operating conditions in Alberta.

[20] L. Gaipl, T. Jaravel, Q. Douasbin, and T. Poinsot. LES of the combustion efficiency of wake stabilized methane jet flames in crossflow. 273:113916.

[21] Global Monitoring Laboratory, NOAA. Co_2 trends. `https://gml.noaa.gov/ccgg/trends/`.

[22] Global Monitoring Laboratory, NOAA. Ch_4 trends. `https://gml.noaa.gov/ccgg/trends_ch4/`.

[23] L. Kostiuk, M. Johnson, and G. Thomas. University of alberta flare research project: final report november 1996 - september 2004. 2. ed. Technical report, University of Alberta, 2004.

[24] [FirstName] Johnson. Oil & gas 5 dec '08: [flare efficiency & emissions: Past & current research]. Technical report, Global Methane Initiative, 2008.

6. Annex: data sets

The data presented in this section is organized as follows:

- Each table correspond to a given flare diameter, a given state of the pilot flame (ON/OFF) and a given state of the wind shield (ON/OFF).
- Inside a table, each line between two horizontal separators correspond to a given Air flow rate
- Between two horizontal separators, only the Natural Gas flow rate in the flare is varied.

ID units	$\dot{m}^{Air}$ [t/h]	$\dot{m}^{NG,f}$ [g/s]	$X^{BG}_{CH_4}$ [ppm]	$X^{BG}_{CO_2}$ [ppm]	X^{BG}_{CO} [ppm]	CI^{M1E} [%]	DI^{M1E} [%]	CI^{M2E} [%]	DI^{M2E} [%]
089	113.0	20.0	50.0	1605	12.2	5.37	4.38	5.76	4.69
090	113.0	10.0	39.4	1045	8.9	7.73	6.37	8.70	7.17
091	113.0	5.0	36.1	753	6.8	12.54	10.63	14.94	12.67
092	113.0	2.5	31.5	605	5.8	19.02	16.15	24.32	20.65
093	113.0	1.0	22.1	522	4.5	24.65	20.44	35.94	29.80
094	80.0	20.0	23.5	2070	6.7	1.82	1.41	1.86	1.45
095	80.0	10.0	24.2	1270	5.8	3.50	2.83	3.66	2.95
096	80.0	5.0	23.4	875	4.9	6.12	5.06	6.69	5.53
097	80.0	2.5	22.7	663	4.2	10.77	9.08	11.98	10.10
098	80.0	1.0	17.5	553	3.5	15.26	12.60	19.40	16.02
099	50.0	20.0	11.7	3045	4.0	0.53	0.38	0.54	0.38
100	50.0	10.0	11.7	1840	3.2	0.93	0.71	1.00	0.76
101	50.0	5.0	13.0	1198	3.0	1.87	1.48	2.14	1.69
102	50.0	2.5	14.1	864	2.7	3.52	2.90	4.31	3.56
103	50.0	1.0	13.0	650	2.5	6.27	5.14	8.41	6.90

Table 11: Results of the combustion tests on the 4 inches flare - pilot ON - wind shield ON.

ID units	$\dot{m}^{Air}$ [t/h]	$\dot{m}^{NG,f}$ [g/s]	$X^{BG}_{CH_4}$ [ppm]	$X^{BG}_{CO_2}$ [ppm]	X^{BG}_{CO} [ppm]	CI^{M1E} [%]	DI^{M1E} [%]	CI^{M2E} [%]	DI^{M2E} [%]
28	113.7	40.0	92.1	2697	22.1	5.21	4.29	5.39	4.43
11	113.7	30.0	87.0	2180	20.0	6.26	5.18	6.67	5.52
12	113.7	20.1	83.4	1620	18.0	8.54	7.14	9.29	7.77
13	113.7	10.0	73.7	1060	16.0	13.55	11.31	15.71	13.11
14	113.7	5.0	52.9	784	13.4	17.07	13.83	20.95	16.97
15	113.7	2.0	29.7	623	10.0	18.23	13.74	24.11	18.16
16	113.7	1.0	20.9	567	8.1	18.54	13.29	25.49	18.27
29	90.0	40.0	74.8	3217	18.5	3.50	2.86	3.46	2.82
30	90.0	30.0	74.0	2525	17.4	4.52	3.72	4.48	3.69
31	90.0	20.0	73.5	1840	16.2	6.48	5.40	6.50	5.42
32	90.0	10.0	69.8	1163	14.7	11.22	9.41	11.69	9.81
33	90.0	5.0	53.8	847	12.9	14.91	12.20	16.71	13.67
34	70.0	40.0	60.4	3985	14.6	2.22	1.81	2.14	1.75
35	70.0	30.0	61.7	3187	14.4	2.89	2.38	2.88	2.37
36	70.0	20.0	60.7	2336	13.4	4.02	3.35	4.15	3.45
37	70.0	10.0	60.1	1460	12.6	7.11	5.96	7.77	6.52
38	70.0	5.0	52.7	1003	11.6	10.87	9.03	12.53	10.40
39	50.0	40.0	50.1	5645	11.3	1.24	1.02	1.24	1.03
40	50.0	30.0	50.0	4356	10.8	1.62	1.35	1.63	1.36
41	50.0	20.0	50.1	3098	10.5	2.37	1.98	2.40	2.01
42	50.0	10.0	47.4	1820	9.9	4.22	3.53	4.32	3.62
43	50.0	5.0	44.9	1205	10.0	7.06	5.84	7.57	6.26
44	30.0	40.0	34.5	9250	9.0	0.51	0.41	0.51	0.41
45	30.0	20.0	38.1	4685	8.5	1.13	0.94	1.09	0.90
46	30.0	5.0	36.6	1720	8.3	3.53	2.90	3.66	3.01
48	11.5	20.0	5.5	11022	3.0	0.06	0.03	0.05	0.02
49	11.5	5.0	9.2	3496	2.7	0.32	0.23	0.29	0.21

Table 12: Results of the combustion tests on the 8 inches flare - pilot ON - wind shield ON.

ID units	$\dot{m}^{Air}$ [t/h]	$\dot{m}^{NG,f}$ [g/s]	$X^{BG}_{CH_4}$ [ppm]	$X^{BG}_{CO_2}$ [ppm]	X^{BG}_{CO} [ppm]	CI^{M1E} [%]	DI^{M1E} [%]	CI^{M2E} [%]	DI^{M2E} [%]
26	113.7	40.0	138.4	2557	28.6	7.99	6.74	8.17	6.90
21	113.7	20.0	110.6	1481	21.0	12.18	10.40	12.84	10.97
20	113.7	10.0	78.7	941	16.0	17.05	14.39	18.30	15.45
19	113.7	5.0	53.4	682	12.8	22.66	18.54	25.14	20.57
18	113.7	2.0	24.3	548	6.8	22.63	17.70	27.80	21.74
17	113.7	1.0	12.5	509	3.8	17.84	13.22	26.17	19.39
50	90.0	40.0	131.4	3192	27.8	5.97	5.02	6.15	5.17
51	90.0	20.0	104.4	1839	20.1	8.88	7.57	9.60	8.18
52	90.0	5.0	58.4	831	13.0	16.40	13.61	21.57	17.90
53	90.0	1.0	18.3	569	5.2	15.11	11.65	32.06	24.72
54	51.4	40.0	125.0	5146	30.0	3.48	2.86	3.40	2.80
55	51.4	15.0	73.8	2258	15.0	5.02	4.24	5.15	4.35
56	51.4	5.0	48.0	1104	9.4	8.42	7.12	9.82	8.30
57	51.4	1.5	30.3	755	8.0	11.12	8.86	21.09	16.79

Table 13: Results of the combustion tests on the 8 inches flare - pilot OFF - wind shield ON.

ID units	$\dot{m}^{Air}$ [t/h]	$\dot{m}^{NG,f}$ [g/s]	$X^{BG}_{CH_4}$ [ppm]	$X^{BG}_{CO_2}$ [ppm]	X^{BG}_{CO} [ppm]	CI^{M1E} [%]	DI^{M1E} [%]	CI^{M2E} [%]	DI^{M2E} [%]
73	113.7	40.0	93.9	2670	22.5	5.37	4.42	5.49	4.52
74	113.7	20.0	63.4	1635	16.1	6.67	5.41	7.23	5.86
75	113.7	10.0	59.4	1060	14.6	11.35	9.25	12.83	10.46
76	113.7	5.0	49.8	777	13.7	16.70	13.30	19.99	15.92
77	113.7	1.0	28.8	561	9.2	24.46	18.65	34.53	26.33
69	90.0	40.0	94.5	3242	21.6	4.32	3.58	4.34	3.60
70	90.0	20.0	59.4	1945	15.5	5.06	4.08	5.37	4.33
71	90.0	10.0	58.0	1233	15.0	8.97	7.24	10.00	8.07
72	90.0	5.0	50.5	873	14.2	13.71	10.87	16.13	12.79
65	70.0	40.0	88.7	3940	19.5	3.25	2.71	3.14	2.62
66	70.0	20.0	59.8	2260	15.0	4.21	3.42	4.18	3.39
67	70.0	10.0	59.5	1394	15.2	7.74	6.26	7.96	6.45
68	70.0	5.0	52.6	990	14.1	11.44	9.17	12.96	10.38
61	50.0	40.0	84.2	5557	17.2	2.11	1.78	2.10	1.77
62	50.0	20.0	65.1	3165	15.8	3.09	2.53	3.24	2.65
63	50.0	10.0	75.4	1855	16.0	6.54	5.48	7.04	5.90
64	50.0	5.0	64.5	1230	14.2	9.69	8.06	11.05	9.19
58	30.0	40.0	64.5	9263	16.9	0.98	0.79	0.99	0.80

Table 14: Results of the combustion tests on the 8 inches flare - pilot ON - wind shield OFF.

ID units	$\dot{m}^{Air}$ [t/h]	$\dot{m}^{NG,f}$ [g/s]	$X^{BG}_{CH_4}$ [ppm]	$X^{BG}_{CO_2}$ [ppm]	X^{BG}_{CO} [ppm]	CI^{M1E} [%]	DI^{M1E} [%]	CI^{M2E} [%]	DI^{M2E} [%]
86	90.0	15.0	75.0	1435	14.1	8.85	7.56	9.07	7.75
87	90.0	5.0	46.6	802	9.2	14.08	11.89	16.68	14.08
82	70.0	40.0	143.0	3910	30.0	5.20	4.38	5.21	4.38
83	70.0	15.0	71.7	1838	13.6	6.20	5.28	6.74	5.75
84	70.0	5.0	47.0	929	8.6	10.79	9.22	12.94	11.05
79	50.0	40.0	146.0	5256	33.2	3.93	3.27	3.84	3.19
80	50.0	15.0	65.0	2280	13.6	4.40	3.69	4.41	3.70
81	50.0	5.0	46.0	1082	8.3	8.24	7.05	9.02	7.71
78	30.0	5.0	30.3	1483	6.6	3.51	2.89	3.56	2.94

Table 15: Results of the combustion tests on the 8 inches flare - pilot OFF - wind shield OFF.

ID	$\dot{m}^{Air}$	$\dot{m}^{NG,f}$	$X^{BG}_{CH_4}$	$X^{BG}_{CO_2}$	X^{BG}_{CO}	CI^{M1E}	DI^{M1E}	CI^{M2E}	DI^{M2E}
units	[t/h]	[g/s]	[ppm]	[ppm]	[ppm]	[%]	[%]	[%]	[%]
213	111.0	61.1	174.9	3931	35.9	6.25	5.29	6.56	5.54
214	111.0	30.6	145.8	2174	29.0	10.00	8.49	10.76	9.14
215	111.0	15.3	112.7	1311	25.2	14.78	12.31	16.60	13.83
216	111.0	3.1	26.4	678	9.4	13.28	9.83	17.50	12.95
212	90.0	61.1	148.2	4770	31.9	4.38	3.67	4.52	3.79
211	90.0	30.6	137.3	2574	26.0	7.77	6.65	8.14	6.96
210	90.0	15.3	107.9	1526	22.5	11.62	9.78	12.73	10.72
209	90.0	3.1	30.3	735	9.9	12.30	9.34	16.13	12.25
205	70.0	61.1	123.5	6172	27.1	2.80	2.34	2.93	2.45
206	70.0	30.6	115.1	3255	22.1	5.08	4.33	5.30	4.52
207	70.0	15.3	103.5	1879	20.6	8.62	7.31	9.41	7.98
208	70.0	3.1	36.0	817	10.6	11.42	8.92	14.75	11.52
204	50.0	61.1	99.2	9159	22.7	1.50	1.24	1.68	1.39
203	50.0	30.6	92.4	4531	18.5	2.87	2.43	3.04	2.57
202	50.0	15.3	91.7	2514	17.5	5.43	4.63	5.90	5.03
201	50.0	3.1	42.9	953	10.7	9.92	8.04	12.27	9.94

Table 16: Results of the combustion tests on the 14 inches flare - pilot ON - wind shield ON.

ID	$\dot{m}^{Air}$	$\dot{m}^{NG,f}$	$X^{BG}_{CH_4}$	$X^{BG}_{CO_2}$	X^{BG}_{CO}	CI^{M1E}	DI^{M1E}	CI^{M2E}	DI^{M2E}
units	[t/h]	[g/s]	[ppm]	[ppm]	[ppm]	[%]	[%]	[%]	[%]
217	111.0	30.6	169.1	2092	33.8	11.95	10.14	12.72	10.80
218	111.0	15.3	131.2	1242	29.6	18.04	15.01	20.05	16.69
219	111.0	3.1	24.4	643	8.7	14.13	10.42	18.64	13.75
220	90.0	3.1	31.8	680	9.7	15.18	11.72	19.42	15.01
221	90.0	15.3	131.6	1434	28.2	15.02	12.60	16.17	13.57
222	90.0	30.6	160.7	2477	31.6	9.44	8.03	9.77	8.31
223	70.0	30.6	148.4	3107	29.4	6.84	5.82	7.01	5.96
224	70.0	15.3	131.1	1750	26.9	11.71	9.89	12.44	10.51
225	70.0	3.1	45.9	737	12.2	17.19	13.77	21.71	17.39
226	50.0	3.1	53.7	851	13.2	14.81	12.07	18.01	14.68
227	50.0	15.3	117.8	2331	22.8	7.55	6.43	7.89	6.72
228	50.0	30.6	133.7	4297	28.5	4.42	3.71	4.55	3.82

Table 17: Results of the combustion tests on the 14 inches flare - pilot OFF - wind shield ON.

7. Annex: Derivation of the formulas for CE and DE

The formulas given in Eq. 4 and Eq. 5 are definitions based on the physical meaning of these quantities. Many terms are implied in these equations but they can be computed from a very limited set of data thanks to atoms conservation and a few hypothesis. The aim of this section is to describe this process.

First let us recall that in the presented setup, two kinds of data are available to compute CE/DE.

- The mass flow rates of Air $\dot{m}^{Air}$ and of Natural Gas $\dot{m}^{NG}$ (including the pilot flame when necessary).
- the molar fraction of CH_4, CO_2 and CO on dry exhaust gases.

These two set of data are quite different for various reasons. The first one is that molar fractions are intensive properties. By contrast the mass flows are extensive. As the CE and DE are also intensive properties, it makes sense to discard the actual size of the system in the following analysis and to focus only on an intensive description of the flow rates by only considering the dilution rate τ_n of the natural gas in the air (see Eq. 2).

Four intensive data are thus available to define only two indicators (CE and DE). There is clearly some over determination in this system and some choices must be made to provide some consistent results. Two approaches will be detailed below:

- The first approach will provide τ_n, CE and DE as functions of $X_{CH_4}^{BG,dry}$, $X_{CO_2}^{BG,dry}$ and $X_{CO}^{BG,dry}$. It is based on the gas analyzer only and does not use data from the flow meters.
- In the second approach the dilution factor τ_n will be computed from the flow meters, and then CE and DE will be functions of τ_n, $X_{CH_4}^{BG,dry}$ and $X_{CO}^{BG,dry}$, i.e. the value of $X_{CO_2}^{BG,dry}$ will not be used directly.

Before starting the derivation, we shall first give a few definition relative to the alkanes, carbon atoms and hydrogen atoms present in the natural gas that will shorten the formulas hereafter:

$$X_{alk}^{NG} = \sum_{k\geq 1} X_{C_kH_{2k+2}}^{NG} \tag{13}$$

$$X_{C-alk}^{NG} = \sum_{k\geq 1} k X_{C_kH_{2k+2}}^{NG} \tag{14}$$

$$X_{H-alk}^{NG} = \sum_{k\geq 1} (2k+2) X_{C_kH_{2k+2}}^{NG} = 2X_{C-alk}^{NG} + 2X_{alk}^{NG} \tag{15}$$

It is then possible to write the molar flux of each species in the burnt gases:

$$\dot{n}_{N_2}^{BG} = \dot{n}^{NG}\left(X_{N_2}^{NG} + \tau_n X_{N_2}^{Air}\right) \tag{16}$$

$$\dot{n}^{BG}_{O_2} = \dot{n}^{NG}\left(\tau_n X^{Air}_{O_2} - \frac{1}{2}(1-\alpha)\left[(2-\beta)X^{NG}_{C-alk} + \frac{1}{2}X^{NG}_{H-alk}\right]\right) \tag{17}$$

$$\dot{n}^{BG}_{C_kH_{2k+2}} = \dot{n}^{NG}\left(\alpha X^{NG}_{C_kH_{2k+2}} + \tau_n X^{Air}_{C_kH_{2k+2}}\right) \tag{18}$$

where only CH_4 is actually present in the air, the other alkanes being totally negligible.

$$\dot{n}^{BG}_{CO} = \dot{n}^{NG}(1-\alpha)\beta X^{NG}_{C-alk} \tag{19}$$

$$\dot{n}^{BG}_{CO2} = \dot{n}^{NG}\left(X^{NG}_{CO_2} + \tau_n X^{Air}_{CO_2} + (1-\alpha)(1-\beta)X^{NG}_{C-alk}\right) \tag{20}$$

$$\dot{n}^{BG}_{H_2O} = \dot{n}^{NG}\frac{1}{2}(1-\alpha)X^{NG}_{H-alk} \tag{21}$$

In all the previous equations, α and β indicate the type and degree of incompleteness as defined in Eq. 3.

The total dry (i.e. without water) molar flux of burnt gases is then:

$$\dot{n}^{BG,dry} = \dot{n}^{BG}_{N_2} + \dot{n}^{BG}_{O_2} + \dot{n}^{BG}_{C_kH_{2k+2}} + \dot{n}^{BG}_{CO} + \dot{n}^{BG}_{CO2} \tag{22}$$

which can be rewritten as:

$$\dot{n}^{BG,dry} = \dot{n}^{NG}\left(\kappa_0 + \kappa_\alpha\alpha + (1-\alpha)\kappa_\beta\beta + \tau_n\right) \tag{23}$$

with:

$$\kappa_0 = X^{NG}_{N_2} + X^{NG}_{CO_2} - \frac{1}{4}X^{NG}_{H-alk} \tag{24}$$

$$\kappa_\alpha = X^{NG}_{alk} + \frac{1}{4}X^{NG}_{H-alk} \tag{25}$$

$$\kappa_\beta = \frac{1}{2}X^{NG}_{C-alk} \tag{26}$$

7.1. Evaluation of CE and DE based on the gas analyzer only

In this situation τ_n, α and β will be evaluated from Eq. 27, Eq. 28 and Eq. 29:

$$X^{BG,dry}_{CH_4} = \frac{\dot{n}^{BG}_{CH_4}}{\dot{n}^{BG,dry}} = \frac{\alpha X^{NG}_{CH_4} + \tau_n X^{Air}_{CH_4}}{\kappa_0 + \kappa_\alpha\alpha + (1-\alpha)\kappa_\beta\beta + \tau_n} \tag{27}$$

$$X^{BG,dry}_{CO} = \frac{\dot{n}^{BG}_{CO}}{\dot{n}^{BG,dry}} = \frac{(1-\alpha)\beta X^{NG}_{C-alk}}{\kappa_0 + \kappa_\alpha\alpha + (1-\alpha)\kappa_\beta\beta + \tau_n} \tag{28}$$

$$X^{BG,dry}_{CO_2} = \frac{\dot{n}^{BG}_{CO_2}}{\dot{n}^{BG,dry}} = \frac{X^{NG}_{CO_2} + \tau_n X^{Air}_{CO_2} + (1-\alpha)(1-\beta)X^{NG}_{C-alk}}{\kappa_0 + \kappa_\alpha\alpha + (1-\alpha)\kappa_\beta\beta + \tau_n} \tag{29}$$

without using the data from the flow meters.

These three equations can be recast in the following system:

$$s_1 + p_1\alpha + q_1(1-\alpha)\beta + r_1\tau_n = 0 \tag{30}$$
$$s_2 + p_2\alpha + q_2(1-\alpha)\beta + r_2\tau_n = 0 \tag{31}$$
$$s_3 + p_3\alpha + q_3(1-\alpha)\beta + r_3\tau_n = 0 \tag{32}$$

where:

$$s_1 = \kappa_0 X_{CH_4}^{BG,dry} \tag{33}$$
$$p_1 = \kappa_\alpha X_{CH_4}^{BG,dry} - X_{CH_4}^{NG} \tag{34}$$
$$q_1 = \kappa_\beta X_{CH_4}^{BG,dry} \tag{35}$$
$$r_1 = \Delta X_{CH_4}^{BG} \tag{36}$$
$$s_2 = \kappa_0 X_{CO}^{BG,dry} \tag{37}$$
$$p_2 = \kappa_\alpha X_{CO}^{BG,dry} \tag{38}$$
$$q_2 = \kappa_\beta X_{CO}^{BG,dry} - X_{C-alk}^{NG} \tag{39}$$
$$r_2 = \Delta X_{CO}^{BG} \tag{40}$$
$$s_3 = \kappa_0 X_{CO_2}^{BG,dry} - X_{C-alk}^{NG} \tag{41}$$
$$p_3 = \kappa_\alpha X_{CO}^{BG,dry} + X_{C-alk}^{NG} \tag{42}$$
$$q_3 = \kappa_\beta X_{CO}^{BG,dry} + X_{C-alk}^{NG} \tag{43}$$
$$r_3 = \Delta X_{CO_2}^{BG} \tag{44}$$

and $\Delta X_k^{BG} = X_k^{BG} - X_k^{Air}$ is the air-corrected measure of species k in the burnt gases.

The β terms can be eliminated quite easily and the following simpler system is obtained:

$$(s_1q_2 - s_2q_1) + (p_1q_2 - p_2q_1)\alpha + (r_1q_2 - r_2q_1)\tau_n = 0 \tag{45}$$
$$(s_2q_3 - s_3q_2) + (p_2q_3 - p_3q_2)\alpha + (r_2q_3 - r_3q_2)\tau_n = 0 \tag{46}$$

This linear system can then be inverted without difficulty to provide α and τ_n. The evaluation of β follows directly, for example starting from Eq. 31:

$$\beta = -\frac{s_2 + r_2\tau_n + p_2\alpha}{q_2(1-\alpha)} \tag{47}$$

After tedious computations, one can show that the dilution rate can be approximated by:

$$\tau_n \approx \frac{X_{CH_4}^{NG} X_{C-alk}^{NG}}{X_{CH_4}^{NG}\left(\Delta X_{CO}^{BG} + \Delta X_{CO_2}^{BG}\right) + X_{C-alk}^{NG}\Delta X_{CH_4}^{BG}} \tag{48}$$

in the limit of high dilutions.

Still in this limit, it can be proven that:

$$\alpha \approx \frac{X^{NG}_{C-alk}\Delta X^{BG}_{CH_4}}{X^{NG}_{CH_4}\left(\Delta X^{BG}_{CO}+\Delta X^{BG}_{CO_2}\right)+X^{NG}_{C-alk}\Delta X^{BG}_{CH_4}} \tag{49}$$

$$\beta \approx \frac{\Delta X^{BG}_{CO}}{\Delta X^{BG}_{CO}+\Delta X^{BG}_{CO_2}} \tag{50}$$

which is the expected limit behavior.

7.2. Hybrid approach for CE and DE based on flow meters and gas analyzer

In this situation, the evaluation of τ_n is performed directly from the flow meters:

$$\tau_n = \frac{W_{Air}}{W_{NG}}\frac{\dot{m}^{Air}}{\dot{m}^{NG}} \tag{51}$$

Only Eq. 27 and Eq. 28 are thus necessary and τ_n is not an unknown anymore. The associated 2x2 system is:

$$t_1 + p_1\alpha + q_1(1-\alpha)\beta = 0 \tag{52}$$

$$t_2 + p_2\alpha + q_2(1-\alpha)\beta = 0 \tag{53}$$

where:

$$t_1 = s_1 + \tau_n r_1 \tag{54}$$

$$t_2 = s_2 + \tau_n r_2 \tag{55}$$

The solution of this system is:

$$\alpha = \frac{t_2 q_1 - t_1 q_2}{p_1 q_2 - p_2 q_1} \tag{56}$$

$$\beta = -\frac{t_1 + p_1\alpha}{q_1(1-\alpha)} \tag{57}$$

One can easily verify that in the limit of high dilutions, a good approximation for α is given by:

$$\alpha \approx \tau_n \frac{\Delta X^{BG}_{CH_4}}{X^{NG}_{CH_4}} \tag{58}$$

When evaluating τ_n with Eq. 48, one finds again:

$$\alpha \approx \frac{X^{NG}_{C-alk}\Delta X^{BG}_{CH_4}}{X^{NG}_{CH_4}\left(\Delta X^{BG}_{CO}+\Delta X^{BG}_{CO_2}\right)+X^{NG}_{C-alk}\Delta X^{BG}_{CH_4}} \tag{59}$$

which is identical to Eq. 49.

7.3. Summary

Two methods are available to compute CE/DE from the experimental data:

- Method 1: The CE, DE and dilution rate are computed from the concentrations of CO, CO_2 and CH_4 provided by the gas analyzer. The flow rate computed with this method is thus potentially inconsistent with the flow meters.
- Method 2: the dilution rate is computed from the flow meters. The CE and DE are the computed from this value and the concentrations of CH_4 and CO only.

Method 1 is interesting since it is based on concentration measurements in the burnt gases only and thus does not require any flow rate. It is usually more consistent when the concentration are high, i.e. at low dilution. Method 2 is useful at high dilution rates since it is less affected by measurement uncertainties at low gas concentrations.

The only source of discrepancy between these two approximations is the lack of consistency between the experimental measurements of flow rates and concentrations. Both methods actually provide identical results on α and β when the dilution rate computed from the flow meters and from the concentrations are identical.

Based on these two methods, four sets of CE/DE/dilution rates can thus be computed:

1. Method 1 Exact (M1E): A 2x2 linear system (Eq. 45 and Eq. 46) must be solved to find α and τ_n and then β can be computed from Eq. 47.
2. Method 2 Exact (M2E): τ_n is computed from Eq. 2 and then Eq. 56 and Eq. 57 provide values for α and β.
3. Method 1 Approximate (M1A): Eq. 49 and Eq. 50 provide good approximations of α and β in the limit of high dilution.
4. Method 2 Approximate (M2A): the downside of Method 2 is that there is no simple approximation for β (since the data on CO_2 can not be used). Equation 58 can however be used for α.

The Fig. 12 to Fig. 14 show the differences between those methods on the 8 inches flare in the optimal setup (data in Tab. 12) with the Exact Method 1 serving as the reference to compare the other methods. The coefficients of a linear fit are shown in Tab.18.

It is seen that Exact Method 1 and Approximate Method 1 are in excellent agreement in all situations: this was expected since the dilution rates are always larger than 100.

On the other hand, the Exact Method 2 provides slightly different results which is also expected since it relies on an independent measure of the mass flows. The difference remains however limited: this is just another confirmation of the consistency of our measurement campaign. The difference is more important in the regions were the dilution rate is important, i.e. for low concentrations of CH_4 and CO_2. In this situation, the relative precision of the gaz analyzer is lower and Method 2 should probably be preferred over Method 1.

Variables	Relation	Slope	Intercept	R^2
α	α_{M2E} vs. α_{M1E}	1.2608	-6.47×10^{-3}	0.9837
	α_{M1A} vs. α_{M1E}	0.9997	8.77×10^{-7}	1.0000
β	β_{M2E} vs. β_{M1E}	1.4006	-2.75×10^{-3}	0.9879
	β_{M1A} vs. β_{M1E}	0.9997	-3.87×10^{-7}	1.0000
$\log(\tau_n)$	$\tau_{n,ME2}$ vs. $\tau_{n,M1E}$	1.0870	-0.513	0.9986
	$\tau_{n,M1A}$ vs. $\tau_{n,M1E}$	1.0019	-0.015	1.0000

Table 18: Consistency check between the methods for α, β and τ_n. M1E = Method 1 Exact. M2E = Method 2 Exact. M1A = Method 1 Approximate.

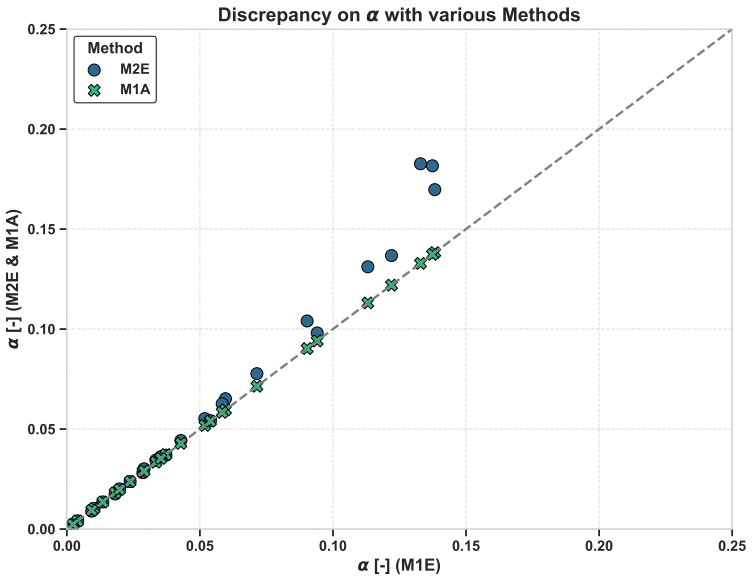

Figure 12: Comparison of α computed with Method 1 Exact, Method 1 Approximate and Method 2 Exact.

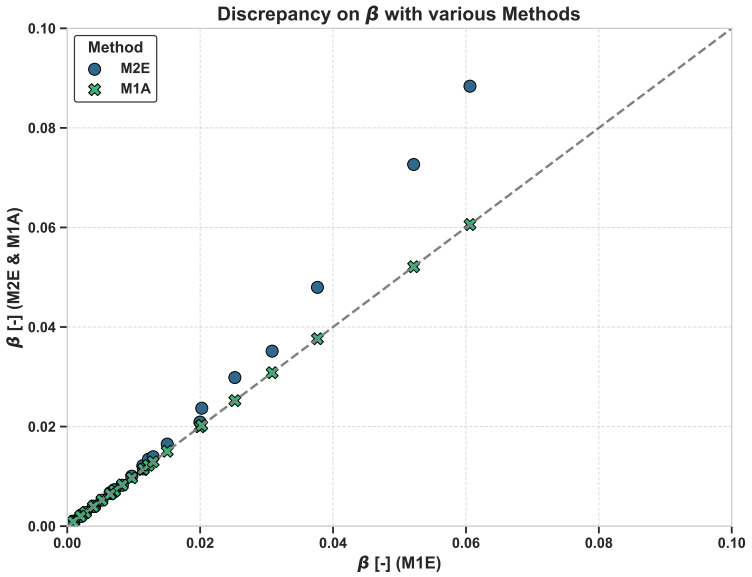

Figure 13: Comparison of β computed with Method 1 Exact, Method 1 Approximate and Method 2 Exact.

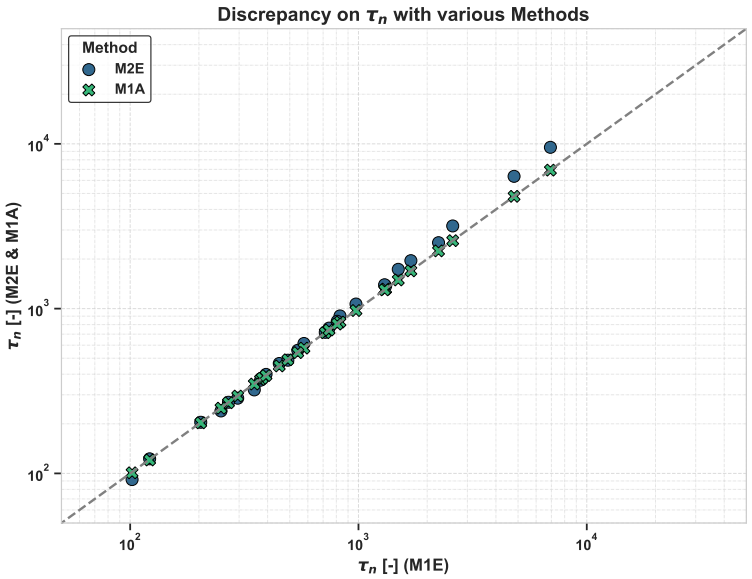

Figure 14: Comparison of τ_n computed with Method 1 Exact, Method 1 Approximate and Method 2 Exact.

8. Annex: Horiba VA-5111 certification

TRE00545C(1/1)

TEST REPORT

1. Specification

Model	VA-5111		HGS No.	WM8TSBRK
Power Source	AC100-240V, 50/60Hz		Output	----
Component	1	CH_4	0～ 100/1000	ppm
	2	CO	0～ 50/500	ppm
	3	CO_2	0～ 1000/10000	ppm

2. Inspection Results

1) External Structure Check ..... Good

2) Operation Function Check ..... Good

3) Performance Check <%FS : % of full scale>

(A) Linearity Check ..... Good

Component No.	Lowest Range			Highest Range		
	Deviation(%FS)	Standard	Gas conc.	Deviation(%FS)	Standard	Gas conc.
1	0.2	±1.0%FS	98.18 ppm	0.3	±1.0%FS	1000 ppm
2	0.1	±1.0%FS	49.8 ppm	0.2	±1.0%FS	480.1 ppm
3	0.4	±1.0%FS	964 ppm	0.3	±1.0%FS	9516 ppm

(B) Repeatability ..... Good

<Zero>

Component No.	1st time(%FS)	2nd time(%FS)	3rd time(%FS)	Average (%FS)	Max. Def. (%FS)	Standard
1	0.4	0.3	0.3	0.3	0.1	±0.5%FS
2	0.5	0.4	0.5	0.5	-0.1	±0.5%FS
3	0.3	0.3	0.2	0.3	-0.1	±0.5%FS

<Span>

Component No.	1st time(%FS)	2nd time(%FS)	3rd time(%FS)	Average (%FS)	Max. Def. (%FS)	Standard	Gas conc.
1	98.2	98.3	98.2	98.2	0.1	±0.5%FS	98.18 ppm
2	99.2	99.4	99.5	99.4	-0.2	±0.5%FS	49.8 ppm
3	96.5	96.5	96.6	96.5	0.1	±0.5%FS	964 ppm

(C) Noise level ..... Good

Component No.	Zero Noise		Span Noise		Gas conc.
	Results (%FS)*	Standard*	Results (%FS)*	Standard*	
1	0.4	1.0%FS	0.5	1.0%FS	98.18 ppm
2	0.3	1.0%FS	0.4	1.0%FS	49.8 ppm
3	0.2	1.0%FS	0.3	1.0%FS	964 ppm

*) Peak to Peak *) Peak to Peak

(D) Response time test ..... Good

<Calibration gas line>

Component No.	90% response (T_{90})		95% response (T_{95})		Flow Rate	Gas conc.
	Results (s)	Standard	Results (s)	Standard	(L/min)	
1	19	≦30s	20	≦45s	0.5	98.18 ppm
2	19	≦30s	21	≦45s	0.5	49.8 ppm
3	18	≦30s	20	≦45s	0.5	964 ppm

(E) Drift test ..... Good

Component No.	Zero Drift			Span Drift			Gas conc.
	Results		Standard	Results		Standard	
1	0.2	%FS/day	±1.0%FS/day	-0.4	%FS/day	±1.0%FS/day	98.18 ppm
2	0.4	%FS/day	±2.0%FS/day	-1.1	%FS/day	±2.0%FS/day	49.8 ppm
3	0.2	%FS/week	±2.0%FS/week	1.9	%FS/week	±2.0%FS/week	964 ppm

(F) Interference ..... Good

<Standard>

Component No.	Intf. gases	H_2O 5.0degC sat.		CO_2 15 vol%		C_3H_8 1000 ppm		CO 1000 ppm	
1	Standard	±2.0	%FS	±4.0	%FS	---		±2.0	%FS
2	Standard	±2.0	ppm	±2.0	%FS	±2.0	%FS	---	
3	Standard	±2.0	%FS	---		±2.0	%FS	±1.0	%FS

<Results>

Component No.	Intf. gases	H_2O 5.0degC sat.		CO_2 15 vol%		C_3H_8 1000 ppm		CO 1000 ppm	
1	Results	0.4	%FS	-0.8	%FS	---		-0.4	%FS
2	Results	0.3	ppm	0.2	%FS	1.4	%FS	---	
3	Results	1.0	%FS	---		0.4	%FS	0.2	%FS

(G) Influence of Flow Rate Variation ..... Good

Component No.	0.5 - 0.3L/min (%FS)	0.5 - 0.7L/min (%FS)	Standard	Gas conc.
1	-0.6	0.4	±1.0%FS	98.18 ppm
2	-0.3	0.3	±1.0%FS	49.8 ppm
3	-0.4	0.4	±1.0%FS	964 ppm

4) Leakage test ..... Result -100 Pa ..... Good
(within -490Pa when pressurized at 49±1kPa for 5 minutes)

5) Insulation resistance test ..... before withstand voltage test 2000 MΩ ..... Good
(More than 5MΩ by use of DC 1000V Megger) after withstand voltage test 2000 MΩ

6) Withstand voltage test ..... Good
(Between AC-E by AC1400V for 5 seconds, no device should be damaged)

7) Accessories check (Quality, quantity and appearance) ..... Good

3. Overall inspection ..... Passed

Date: 21 Nov 2024 Inspector: T. Toyosaka Approver: H. Nishihara

HORIBA, Ltd.

Figure 15: Results of the calibration tests


HORIBA

検 査 票
TEST CERTIFICATE

当社の製品は、品質保証の国際規格ＩＳＯ ９００１の品質システム【審査機関：（財）日本品質保証機構（登録証№ ＪＱＡ－０２９８）】に従い生産されており、定められた作業標準及び検査規格に基づく適切な品質管理及び検査が行なわれ、結果は仕様を満足しております。

We certify that this product is thoroughly inspected and confirmed to meet all of its necessary criteria specified in Inspection Standard.
HORIBA LTD is operating a Quality Management System which complies with all of the requirements of ISO 9001.(Certificate Number JQA-0298)

検査者
INSPECTOR
氏名：
NAME T. Tayonaka

検査責任者
SUPERVISOR
氏名：
NAME H. Nishikawa

HORIBA Ltd. Kyoto Japan
Quality Control Dept.
株式会社 堀場製作所

Figure 16: Certificate from Horiba